Cement and Concrete Composites 146 (2024) 105344

Contents lists available at ScienceDirect

Cement and Concrete Composites

journal homepage: www.elsevier.com/locate/cemconcomp

The effect of varying cement replacement level on alkali metal distribution in cement pastes

Petter Hemstad [a,*], Barbara Lothenbach [a,b], Knut Ose Kjellsen [c], Klaartje De Weerdt [a]

[a] Department of Structural Engineering, NTNU, Trondheim, Norway
[b] Laboratory for Concrete & Asphalt, Empa Dübendorf, Switzerland
[c] Heidelberg Materials Sement Norge AS, Brevik, Norway

ARTICLE INFO

Keywords:
Pore solution
Alkali-aggregate reaction
Temperature
Calcium-Silicate-Hydrate (C–S–H)
Supplementary cementitious materials (SCM)

ABSTRACT

This study investigates how the level of Portland cement (PC) replacement affects the distribution of alkali metals in cement pastes, and how this relates to alkali silica reaction (ASR). Pore solution and hydrates were analysed for pastes with 22 % and 35 % PC replaced with limestone, fly ash (FA), and volcanic pozzolan (VP), cured for 180 days at 20, 38, and 60 °C. A significant portion of Na in VP is likely bound in non-reactive minerals. Curing temperature had limited effect on the distribution, mostly related to increased reaction of FA and VP. Higher replacement level increased pore solution volume and decreased concentration of K, but not of Na. It also did not change the amount of Na and K bound by C-A-S-H, as less C-A-S-H formed while (Na,K)/Si ratios increased to compensate. Adding more SCM did not lead to more reacted SCM, thus the additional SCM mainly acted as filler.

1. Introduction

The alkali-silica reaction (ASR) is a major deterioration mechanism for concrete. The alkali in the concrete pore solution can react with reactive silica species in aggregates to form an expansive gel leading to the expansion of the concrete [1]. Expansion of concrete members in structures such as bridges and dams can lead to distortion of the structure, and build-up of local stresses the structure was not dimensioned for. This can endanger the structural integrity, giving rise to costly repairs, decommissioning, or in worst-case structural failure [2]. ASR is pervasive and has been identified in most corners of the world [3]. Due to its massive scale and risk, it is important that we fully understand the mechanisms behind ASR, to be able to design concrete for future structures with minimal risk of ASR.

ASR occurs through the pore solution. It is therefore likely that better understanding of the pore solution composition can improve understanding of ASR [4]. The pore solution is in equilibrium with the solid phases of the cement paste and aggregates, which means that a thorough understanding requires that both the liquid and solid phases are investigated. Of particular importance for ASR is how the alkali metals Na and K that participate in the reaction are distributed. One hypothesis is that only the alkali metal ions in solution are contributing to the initiation of ASR, whereas those that are physically or chemically bound in solid phases do not.

There are at present open questions regarding the role of aggregates in the alkali metal balance. Aggregates can be both a source and a sink of Na and K [5], whilst the formation of ASR gel might at first serve as a sink, but could gradually release alkali metals again [6]. Rivard et al. [7,8] investigated how alkali metals are distributed in concrete, accounting for leaching, but the compounding uncertainty in studying such a complex system are quite large. With the uncertainty of alkali metals taken up by aggregates and gel, they had to make assumptions regarding the amount bound by C-A-S-H. The present study focuses on the distribution of Na and K in the cement paste, as understanding the cement paste system is the starting point for future studies of the more complex concrete system. We consider the alkali metals to distribute between four main parts: non-reactive mineral phases, unreacted phases, adsorbed on C-A-S-H, and free in the pore solution.

The interactions between pore solution and hydrates have been studied using a variety of approaches. Chen and Brouwers [9] calculated the chemical binding of Na and K in C-A-S-H using literature data, focusing on a composite cement with slag. They assumed that there was a correlation between the concentration of Na and K in solution and the amount bound by C-A-S-H and found that binding of Na was close to linear whereas K followed a Freundlich isotherm. Taylor [10] proposed a model to calculate the Na and K distribution in hydrated Portland

* Corresponding author. Richard Birkelands vei 1A, 7491, Trondheim, Norway.
E-mail address: petter.hemstad@ntnu.no (P. Hemstad).

https://doi.org/10.1016/j.cemconcomp.2023.105344
Received 29 May 2023; Received in revised form 14 September 2023; Accepted 18 October 2023
Available online 30 October 2023

cement paste and fly ash containing cement paste. He assumed separate linear binding isotherm for Na and K and accounted for variations in the replacement level of fly ash. These are examples of why it is important for ASR studies to report Na and K separately, rather than obscuring them with the common "sodium equivalent" (Na_2O_{eq}) [10].

Chappex and Scrivener [11] investigated a series of composite cement pastes to see the effect of the composition of C-A-S-H on physical binding of Na and K. They found that at similar Ca/Si-ratios, C-A-S-H with higher content of Al bound significantly more alkali metals than those with lower Al content. However, this was only true for Ca/Si < 1.2, as for Ca/Si 1.5 there was almost no difference between a C-A-S-H and a C–S–H with no Al. They suggested therefore that there must be some other mechanism than increasing Al/Ca-ratio that makes alumina-rich supplementary cementitious materials (SCMs) good at mitigating ASR.

Another approach to measure alkali binding is to use synthetic C-A-S-H in suspensions. Hong and Glasser documented that lower Ca content and/or more Al in C-A-S-H increases the negative surface charge, thereby increasing the adsorption of alkali metal cations [12,13]. L'Hôpital et al. [14] synthesized C-A-S-H with various Ca/Si ratios in the range 0.6–1.5, and found a strong increase in binding with decreasing Ca/Si ratio. Similarly to Chappex and Scrivener [11] they also reported that the Al/Si had little impact on alkali metal binding. More recently Yan et al. [15] investigated a large range of synthetic C-A-S-H compositions (Ca/Si range 0.6–1.2) and reported close correlation between decreasing Ca/Si ratio and increasing alkali uptake in C-A-S-H.

In a previous study Hemstad et al. [16] investigated how alkali metals distribute in hydrated cement pastes containing SCMs and limestone. They determined how Na and K distribute between the pore solution, physically bound through adsorption on calcium-aluminium-silicate-hydrates (C-A-S-H), and chemically bound as parts of non-reactive and unreacted phases. The cement pastes in that study were a Portland cement (PC), PC replaced with 22 % limestone, and PC replaced with 18 % of two supplementary cementitious materials (SCMs) plus 4 % limestone. The investigated SCMs were a fly ash (FA), which has been traditionally used in Norway as a mitigation measure for ASR, and a volcanic pozzolan (VP), which might partially replace FA in composite cements for the Nordic market. The cement pastes were cured for 180 days at 20, 38, and 60 °C to study the effect of temperature and the partial replacement of clinker with other materials on the alkali distribution in cement paste, thus expanding on the work of Taylor [10] and Duchesne and Bérubé [17]. The conclusions were that for PC cured in sealed containers at 20 °C, Na and K distribute evenly between pore solution and C-A-S-H. Partial replacement with limestone did not greatly influence the distribution, but mainly diluted the alkali metal concentration in the pore solution. Using pozzolanic SCMs resulted in a larger share of Na and K being bound by C-A-S-H. This agreed with other studies, such as the one by Duchesne and Berube [18] that demonstrated how some SCMs reduce the concentrations of (Na + K) despite containing more Na and K than the clinker. Elevating the curing temperature had little effect on the distribution of the alkali metals, except for the pastes with SCMs. At 60 °C the accelerated pozzolanic reaction leads to more C-A-S-H with lower Ca/Si ratio that binds more Na and K.

A limitation of the previous study by Hemstad et al. [16] was that only one level of replacement was included. A commonly observed aspect with using SCMs to suppress ASR is that higher replacement levels are more effective [18–20]. This has been correlated to the formation of more C-A-S-H with lower Ca/Si ratio. This C-A-S-H binds more Na and K, thereby lowering the concentration of alkali metals in the pore solution. The same change also reduces the concentration of OH^-, which can potentially make the dissolution of silica and formation of alkali silica gel thermodynamically unfavourable or kinetically slow.

This paper investigates the alkali metal distribution based on the pore solution composition and volume, together with the degree of reaction (DoR) of the SCMs and PC, amount and composition of C-A-S-H at two different SCM contents (22 and 35 wt%). The dilution effect and pozzolanic effect are distinguished through comparison with a plain PC reference as well as 22 and 35 wt% limestone cement references. We also evaluate the effect of elevating the curing temperature from 20 to 38 and 60 °C, which are temperatures typically used for accelerated performance testing. The goal is thereby to determine how higher level of PC replacement changes the distribution of Na and K between the pore solution, C-A-S-H, unreacted phases, and non-reactive phases. In turn, these differences are related to expansion of concrete caused by ASR during accelerated tests.

2. Methods and materials

The present work builds upon a previous publication by Hemstad et al. [16]. It utilizes the same methods and materials, and we have therefore limited the level of detail here. Differences between the two studies are highlighted in the text. Fig. 1 shows the experimental flow chart used to determine the alkali metal distribution, reprinted from Ref. [16].

As a convention for this study, "cement" is used to refer to any of the blended/composite cements in Table 4. Any result presented as "per 100 g cement" is normalized to the amount of blended/composite cement, not to the amount of clinker or Portland cement.

2.1. Raw materials

The raw materials in this study were a Portland cement (PC), limestone (L), fly ash (FA), and a volcanic pozzolan (VP). They were characterized using X-ray fluorescence (XRF) and quantitative X-ray diffraction with Rietveld refinement (QXRD). The particle size distribution and Blaine specific surface were also determined. Table 1 shows the oxide composition of the materials as determined by XRF, together with median particle size (d_{50}) and Blaine specific surface. Table 2 gives the QXRD characterization of the PC, whilst Table 3 gives the QXRD characterization of the L, FA, and VP. It is here important to note that the QXRD is unable to determine the exact composition of many of the mineral phases that can form solid solutions. As such we had to make an assumption regarding their compositions, and therefore chose to use the average composition such that (Na_x,K_x) would be ($Na_{0.5}$,$K_{0.5}$).

2.2. Cement paste preparation

Table 4 shows an overview of the cement pastes cast for this study. A reference was cast using 100 % PC. Two series of pastes were made, one with 22 % and another with 35 % total replacement of PC with other materials. The mass percent of each component other than PC is given in the shorthand name. The pastes are as following: PC with partial replacement with limestone (22L and 35L), PC with replacement with fly ash and limestone (18FA-4L and 25FA-10L), and finally PC with replacement by a natural volcanic pozzolan and limestone (18VP-4L and 25VP-10L). In some figures the pastes with the same ingredients with different levels of replacement are compared. In these cases, a simplified labelling is used, with indication of replacement level also included. The simplified labelling is PC-L for 22L and 35L; PC-FA for 18FA-4L and 25FA-10L; PC-VP for 18VP-4L and 25VP-10L.

For each paste, 750.0 g composite cement was made by weighing the cement components in individual steel bowls, then combining them in a larger bowl and mixing with a steel spoon. 375.0 g deionized water was then weighed into a Braun shear mixer (water/binder 0.500), then the cement was spooned into the water. The pastes were mixed at medium speed (setting 6/15) for 1 min, then the walls of the bowl were scraped, before the mixture was blended for 1 more minute.

The mixed cement pastes were spooned into 125 mL polyethylene bottles and deposited into 30 mL snap-lock bottles using a 50 mL syringe. These were closed with lids and parafilm, then placed in water baths and cured for 180 days at 20, 38, and 60 °C. The 125 mL bottles had water up to their bottle necks, whereas the 30 mL bottles were submerged.

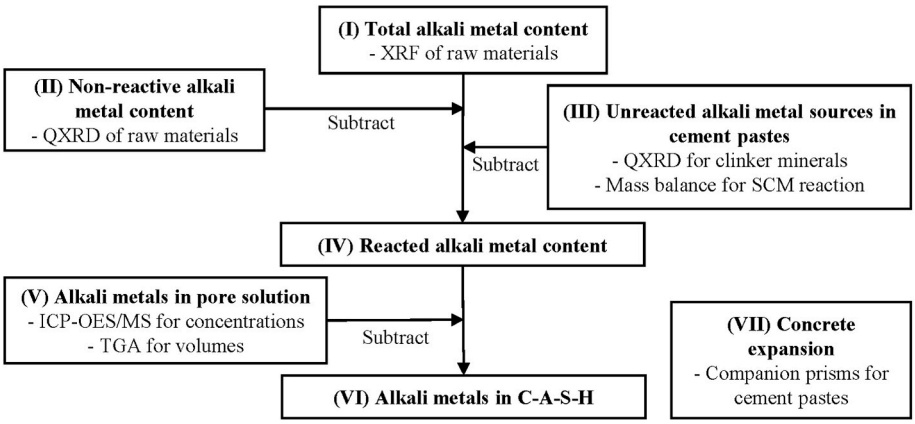

Fig. 1. Flow chart of the experimental process to determine the alkali metal distribution, reprinted from Ref. [16].

Table 1
Characterization of the Portland cement (PC, fly ash (FA), volcanic pozzolan (VP), and limestone (L). Included are element compositions determined by XRF given as oxides, median particle size (d_{50}) and mass specific Blaine surface area.

Material	PC [wt%]	FA [wt%]	VP [wt%]	L [wt%]
SiO_2	19.61	55.07	47.37	13.21
Al_2O_3	4.72	21.55	13.71	3.33
TiO_2	0.34	0.94	1 54	0.17
MnO	0.06	0.06	0.17	0.15
Fe_2O_3	3.17	7.04	12.38	1.86
CaO	63.14	5.26	11.23	44.35
MgO	2.30	2.23	10.76	1.68
K_2O	1.10	2.10	0.26	0.75
Na_2O	0.40	0.92	1.70	0.23
SO_3	3.72	0.17	0.11	0.60
P_2O_5	0.11	0.71	0.18	0.04
LOI 950 °C	1.30	–	–	–
LOI 1050 °C	–	3.30	0.24	33.42
Sum	**99.97**	**99.35**	**99.64**	**99.79**
d_{50} [μm]	12.4	11.3	5.1	16.1
Blaine surface [m^2/kg]	453	450	733	402

Table 2
Quantitative XRD Rietveld analysis of the Portland cement (PC) used in this study. These materials were all considered as reactive in the mass balance.

Mineral	Pure mineral composition	PC [wt%]
Alite – C_3S	Ca_3SiO_5	60.4
Belite – C_2S	Ca_2SiO_4	14.4
Aluminate – C_3A	$Ca_3Al_2O_5$	7.7
Ferrite – C_4AF	$Ca_4(Al,Fe)_2O_6$	8.8
Arcanite	K_2SO_4	0.2
Aphthitalite	$NaK_3(SO_4)_2$	1.5
Ca-Langbeinite	$Ca_2K_2(SO_4)_3$	0.2
Periclase	MgO	1.2
Lime	CaO	0.4
Portlandite	$Ca(OH)_2$	0.6
Sum of clinker phases		**95.5**
Anhydrite	$CaSO_4$	0.8
Bassanite	$CaSO_4 \cdot ½H_2O$	2.9
Gypsum	$CaSO_4 \cdot 2H_2O$	0.4
Sum of set regulators		**4.1**
Calcite	$CaCO_3$	0.4
Sum		**100.0**

2.3. Concrete expansion

The corresponding concrete prisms were cast and monitored for expansion according to the Norwegian Concrete Prism test (NCPT, 38 °C [21]) and RILEM AAR-11 CPT (60 °C [22]). The NCPT is similar to RILEM AAR-10 [23] with small deviations in the concrete composition. The same cements as for the cement pastes were used, making concretes with 445–450 kg/m^3 cement and w/c ratio 0.48. All cements were tested except for those with 35 % replacement at 60 °C. A blend of unreactive sand (0/4 mm), reactive sand (0/10 mm) and reactive gravel (4/16 mm) was used. The reactive gravel was from Ottersbo and is used as a reference aggregate to test ASR mitigating properties of composite cements in Norway. The reactive sand was from Søberg. Detailed description of the concrete compositions is given as supplementary data to this paper, or can be found in Hemstad et al. [16].

The 38 °C prisms were stored at 20 °C in air at 100 % RH for 24 h, then 30 min in water before the reference length was measured. They were then stored over water at 100 % RH and 38 °C for 1 year. Length measurements were performed after storing the prisms for 12–20 h at 20 °C.

The 60 °C prisms were also pre-cured at 20 °C for 24 h at 100 % RH, before being moved to containers in a 60 °C climate chamber with 100 % RH. The reference length was determined after 24 h of storage at 60 °C. The length measurements were performed at 20 °C without pre-cooling the prisms.

2.4. Liquid analyses

The 125 mL bottles were used for pore solution expression. For each cement paste at each temperature, three parallel samples were pressed and analysed. They were placed in a pore solution expression kit mounted in a hydraulic press. A 150 MPa pressure was applied for 10 min, then the pressure was increased to 255 MPa until 3–8 mL of liquid was extracted. 1 mL of the pore solution was pipetted out and diluted 1:100 with deionized water. 10 mL of this diluted solution was acidified with 140 μL 32.5 % HNO_3, for a total dilution of 1:101.4 with a final concentration of 0.1 mol/L HNO_3. ICP-OES/MS was performed at Heidelberg Cement Global R&D for PC and the pastes with 22 % replacement, and ICP-MS for 35 % replacement was performed at the Department of Chemistry at NTNU. There can be some issues with repeatability of ICP measurements between labs, which is explained in detail in Ref. [24]. The concentrations of Na, K, S, Si, Al, and Ca were measured.

The concentration of OH^- was calculated using the charge balance in Equation (1):

$$[OH^-] = [Na^+] + [K^+] + 2[Ca^{2+}] - 2[SO_4^{2-}] \quad (1)$$

where *[x]* stands for the concentration of ion *x* in mmol/L.

2–3 mL of the undiluted pore solutions were used to measure pH by pipetting it into a 15 mL centrifuge tube. A WTW SenTix 81 electrode was used to measure the temperature and potential of each solution. All solutions were measured at room temperature (22 ± 1 °C), The potentials were calibrated using KOH solutions with concentrations 0.1, 0.5 and 1 mol/L, according to the method described by Traynor et al. [25].

Table 3
Quantitative XRD Rietveld analysis of the limestone (L), fly ash (FA) and volcanic pozzolan (VP) used in this study. The chemical composition of each phase and whether it was considered as reactive in the mass balance is also included. Phases marked with (*) are solid solutions with undetermined composition, where an average composition was used (i.e., (Na_x,K_{1-x}) becomes $(Na_{0.5},K_{0.5})$. A "-" is used to indicate where a mineral was not detected in the material.

Mineral	Chemical composition	Reactive in mass balance?	Limestone [wt%]	FA [wt%]	VP [wt%]
Calcite	$CaCO_3$	Yes	78.1	0.2	–
Belite – C_2S	Ca_2SiO_4	Yes	–	0.8	
Gypsum	$CaSO_4 \cdot 2H_2O$	Yes	0.8	–	–
Periclase	MgO	Yes	–	1.0	–
Lime	CaO	Yes	–	0.4	–
Portlandite	$Ca(OH)_2$	Yes	–	–	–
Anhydrite	$CaSO_4$	Yes	0.8	–	–
Mullite	$Al_6Si_2O_{13}$	No	–	7.0	–
Quartz	SiO_2	No	5.0	5.9	–
Maghemite	Fe_2O_3	No	–	1.6	–
Hematite	Fe_2O_3	No		0.5	
Anatase	TiO_2	No	–	0.3	–
Microcline	$KAlSi_3O_8$	No	2.3	–	–
Sanidine*	$(K_{0.5},Na_{0.5})$ $Al(Al_{0.5},Si_{0.5})Si_2O_8$	No	1.3	–	
Anorthite	$CaAl_2Si_2O_8$	No	5.2	–	–
Augite*	$(Ca_{0.5},Fe_{0.5})$ $(Mg_{0.5},Fe_{0.5})Si_2O_6$	No	1.9	–	2.8
Diopside*	$Ca(Mg_{0.5}, Fe_{0.5})$ Si_2O_6	No	1.9	–	2.8
Amphibole*	$Ca_2(Mg_{0.5},Fe^{+2}_{0.5})_4$ $Al(Si_7Al)O_{22}(OH_{0.5}, F_{0.5})_2$	No	1.2	–	–
Clinochlore*	$(Mg_{0.5},Fe_{0.5})_6$ $(Si, Al)_4O_{10}(OH)_8$	No	0.7	–	–
Biotite (mica)*	$K(Fe_{0.5},Mg_{0.5})_2$ $(Si_3AlO_{10})(OH)_2$	No	1.3	–	
Aegirine	$NaFeSi_2O_6$	No	–	–	1.1
Forsterite	Mg_2SiO_4	No	–	–	5.0
Albite	$NaAlSi_3O_8$	No	–	–	5.1
Montmorillonite*	$Ca_{0.2}(Al_{0.5},Mg_{0.5})_2$ $Si_4O_{10}(OH)_2 \cdot H_2O$	No	0.3	–	–
Amorphous	–	Yes	–	82.3	83.2
Sum	–	–	100.8	99.9	100.0

Table 4
Overview of the cement pastes cast for this study.

Cement type	Replacement level [wt%]	Shorthand name	PC [wt%]	SCM [wt%]	L [wt%]
Portland cement	0	PC	100	0	0
Portland cement with limestone	22	22L	78	0	22
Fly ash cement	22	18FA-4L	78	18	4
Volcanic pozzolan cement	22	18VP-4L	78	18	4
Portland cement with limestone	35	35L	65	0	35
Fly ash cement	35	25FA-10L	65	25	10
Volcanic pozzolan cement	35	25VP-10L	65	25	10

2.5. Solid analyses

Analysis of the samples were performed according to the practices recommended in Ref. [26]. Slices of cured cement paste were cut out from the middle of the 30 mL bottles using a water-cooled IsoMet 1000 Precision Saw. A 3 mm slice was extracted for analysis with SEM, whilst a 6 mm slice was extracted for TGA and XRD analysis. For TGA and XRD, the paste was first coarsely ground to pass a 1 mm sieve, then placed in a vacuum filtration unit for a double solvent exchange. The ground paste was stirred together with 100 mL 2-propanol, left to rest for 5 min, then filtered dry. This was repeated once more. Then, 20 mL diethyl ether was added and stirred with the paste and left for 5 min. After filtering the ether off and drying the paste, it was transferred to a small plastic container and stored overnight in a vacuum desiccator at −0.2 bar pressure. The overnight storage ensured evaporation of most of the solvents. Finally, the pastes were ground to pass a 63 μm sieve and analysed with TGA and XRD the same day. These pastes are assumed to have no free water, as the solvents have replaced the free water and then evaporated.

The TGA instrument used was a Mettler Toledo TGA/DSC 3+. Around 200 μg of cement paste powder was placed in a 600 μL alumina crucible. It was then heated from 40 to 900 °C at 10 °C/min whilst purging with 50 ml/min N_2. The resulting mass loss curves were used to determine the bound water and Portlandite (CH) content of the cement pastes. Bound water was found as the mass loss between 40 and 550 °C, as we assume that at 550 °C all chemically bound water has evaporated [27]. CH was determined by using a vertical step of the mass loss curve between ca. 420 and 520 °C, based on where the CH peak could be identified in the derivative mass loss curve. These contents were normalized to the amount of cement by multiplying with 100 % and dividing by the remaining mass percentage at 550 °C [27]. A discussion on different methods to assess bound water content can be found in Ref. [28].

In this study the amounts of free and bound water are related by Equation (2).

$$m_{free\ water} = m_{total\ water} - m_{bound\ water} \quad (2)$$

Here m stands for mass. Since all pastes were mixed with w/c ratio 0.5,

we can normalize to 100 g (composite) cement which gives Equation (3).

$$[per\ 100g\ cement] : m_{free\ water} = 50g - m_{bound\ water} \quad 3$$

A Bruker AXS D8 Focus XRD with a Lynxeye detector and CuKα source (λ = 1.54 Å) was used to scan the cement pastes. The dried paste powders were scanned from 5 to 55 °2θ over 45 min with a step size of 0.01 °2θ and step time 0.5 s. A quartzite sample was analysed along each series of scans as an external standard. The standard was used to make a quantitative Rietveld analysis of the pastes.

The 3 mm cement paste slices were used for SEM-EDS analysis. Smaller pieces of 3–4 discs from pastes with the same SCMs were cast in epoxy, then polished using sandpaper and diamond sprays with ethanol lubricant. The surfaces were then carbon coated. A Hitachi S–3400 N Zeiss SUPRA-55 VP SEM was used for imaging. It was equipped with an Oxford Instruments X-Max 80 mm^2 EDS, which was used to determine elemental composition of various points. EDS points were acquired at 15 kV accelerating voltage. Around 100–150 points from inner product and a similar number of points from outer product were collected. Scatter plots of atomic ratios were used to find the composition of C-A-S-H, expressed as Ca/Si, Al/Ca, S/Si, Na/Si and K/Si. These plots are provided in "Appendix C: SEM-EDS".

2.6. Mass balance

The characterization of raw materials, pore solution and hydrate phases were used as input for a mass balance model. This model was used to calculate the distribution of phases in the cement pastes. Using the XRF and QXRD of the raw materials, a reactive composition was found by subtracting the amount of all elements incorporated in unreactive minerals such as for example quartz. These amounts were then subtracted from the reactive composition. The remaining reactive composition was used to sequentially form different phases based on the availability of different elements: Mg formed periclase, Fe formed siliceous hydrogarnet, Si formed C-A-S-H, ettringite was formed based on QXRD of the paste, remaining S formed monosulphate, remaining Al and C formed monocarbonate, leftover C formed calcite, and all remaining Ca formed CH. A degree of reaction for the SCMs was found by minimizing the difference between CH content measured with TGA and calculated with the model. Zuschlag [28] documented in her PhD thesis that for these cement pastes there was good agreement between this mass balance approach and using image analysis for the degree of reaction.

The bound water content from TGA was subtracted from the total added water (50 g/100 g cement) to find the mass and volume of free water (Equation (3)). This volume was multiplied with the measured pore solution concentrations to determine how much of each element should be present in the pore solution.

The results of that mass balance calculations can potentially differ from the real hydrate composition due to the potential carbonation in particular of portlandite during sample preparation and due to the potential underestimation of the alkali content by the XRF measurements (see Ref. [29]), which can lead to an underestimation of alkali content in C-A-S-H.

The amount of Na and K in non-reactive phases (Figs. 16 and 17) were calculated using QXRD of the raw materials (Table 3), where the amounts of each non-reactive mineral in the pastes were multiplied with the composition of that mineral. If a mineral has a solid solution (for example Na_x,K_{1-x}), the average molar formula ($Na_{0.5},K_{0.5}$) was used. As an example of these calculations, VP contains 5.1 wt% albite ($NaAlSi_3O_8$). Multiplying the weight fraction of Na in albite (9 %) with the amount of the mineral means that around 0.45 % of the mass in VP is Na bound in albite. The assumption that phases such as biotite, albite, and sanidine are non-reactive agree with the findings of Kalina et al. [30].

The unreacted fraction of Na and K (Figs. 16 and 17) are composed of unreacted clinker minerals and SCMs. For the clinker minerals and PC composition there was some disagreement between the elemental composition (XRF, Table 1) and mineral composition (QXRD, Table 2) of the PC. To estimate the composition of the clinker minerals, the mineral composition table from Taylor [31] was modified so that the total elemental composition of the PC as determined by XRD and QXRD was equal. This clinker mineral composition was then multiplied with the amount of each clinker mineral remaining in the cement pastes after hydration. Details related to the assumptions made in these calculations as well as the spreadsheet with the calculations are made available on request and are also described in more detail in Ref. [16].

3. Results

3.1. Concrete expansion

Fig. 2 shows the expansion curves for the concrete prisms. At 38 °C, PC, 22L and 35L expand rapidly and exceed the upper expansion limit of 0.03 %. The higher the limestone content and thus the dilution of the PC, the slower is the observed expansion. For both levels of replacement for FA and VP the expansion is below the limit of 0.03 % at 52 weeks. Again, the expansion is lower at 35 % than 22 %. The PC-VP concretes expand slightly more than PC-FA. At 52 weeks 18FA-4L has expanded by 0.005 % and 18VP-4L by 0.014 %. Similarly, 25FA-10L has expanded by −0.001 %, and 25VP-10L by 0.008 %.

At 60 °C, both PC and 22L clearly exceed the 1-year expansion limit of 0.03 % before 16 weeks. 18FA-4L expands slowly, and barely exceeds the limit with 0.032 % expansion at 52 weeks. 18VP-4L exceeds the expansion limit after 26 weeks and has a final expansion of 0.048 %. Both 18FA-4L and 18VP-4L show flattening expansion curves, likely caused by alkali leaching.

The next sections will focus on the differences in the hydrate assemblage, in alkali concentrations and alkali distribution within hydrated cements and their relation to the expansion observed in concrete tests.

3.2. Pore solution

In this section we describe the changes in the pore solution composition for the investigated binders cured at 20, 38 and 60 °C. The values obtained at 20 °C are in the same range as the ones reported by De Weerdt et al. [32] on similar systems, as well as in the review paper on pore solution composition of blended cements by Vollpracht et al. [33]. The impact of the curing temperature is similar to that observed for fly ash cements by Deschner et al. [34], i.e. little effect in most cases, but a clear increase of sulphate concentrations in solution with temperature. There is also a clear trend of increasing Na concentration for the VP pastes with increasing temperature. In this study we will focus on the Na and K concentrations though for the sake of completeness the measured S, Al, Ca, and Si concentrations are presented as well. Only the concentrations of Na, K and S were used in the mass balance, as the amounts of Al, Ca and Si in pore solution were too low to have any real impact on the calculations.

Fig. 3 shows the pH of the pore solutions measured at 22 °C, as recalibrated with KOH solutions according to the method by Traynor et al. [25]. Fig. 4 shows the concentrations of Na, K and S in the pore solutions, together with the calculated concentration of OH^- (Equation (1)). Fig. 5 shows the concentrations of Al, Ca, and Si. Table 6 in "Appendix A: Pore solution data" provides the numbers for these figures.

The pH of all pore solutions tended to decrease with increasing temperature and increasing replacement level. At 20 °C, partial replacement with limestone reduced the pH compared to the pure PC pastes. Increasing temperature to 38 and 60 °C had a similar effect on the limestone pastes as on the PC pastes, though the decrease at 60 °C is larger. The FA and VP pastes had lower pH than the limestone pastes, and increasing replacement level decreased the pH. All these pastes showed similar trends of reduced pH when the temperature was increased to 38 and 60 °C. It is worth to note that all pore solutions have pH above 12.5, which is consistent with the presence of CH in all the

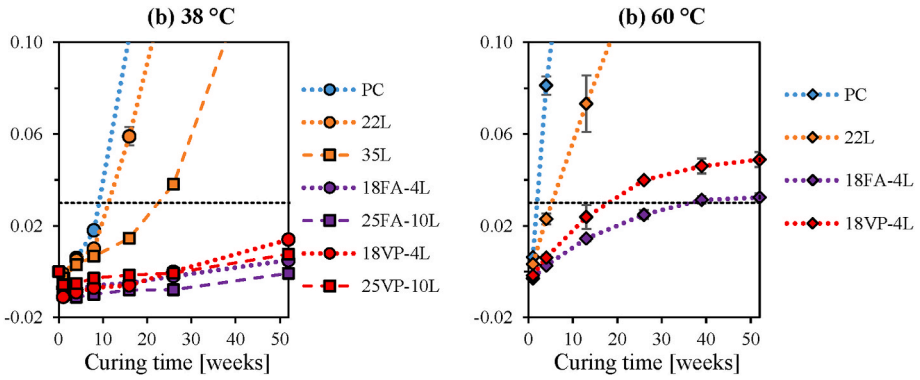

Fig. 2. Expansion curves for concrete prisms cured at 38 °C (a) and 60 °C (b), with the 52 week expansion limit of 0.03 % indicated with a dashed black line.

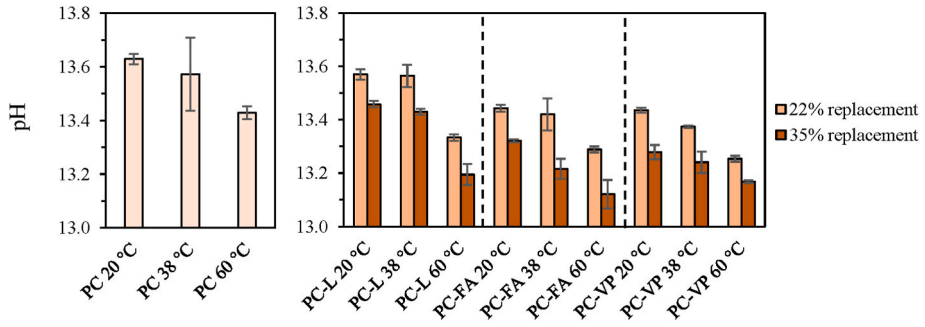

Fig. 3. pH for the pore solutions based on recalibration of the measurements with KOH solutions. All solutions were measured at room temperature around 22 °C.

pastes.

The concentration of Na in the PC pastes was not greatly affected by temperature. Replacing parts of PC with limestone reduced the concentration of Na, with higher replacement causing a greater reduction in concentration. The reduction is not proportional to the replacement level, indicating that the concentration is not only governed by the dilution of PC. Both limestone pastes had small increases in Na concentration with increasing temperature. FA reduced the Na concentration compared to limestone, whereas VP led to an increase. Higher replacement level of FA reduced the concentration further, whereas the Na concentration was similar for both replacement levels with VP. When the curing temperature was increased, there was a small increase in the concentrations of Na in both FA pastes. The largest increase in Na concentration due to increased curing temperature was observed for the PC-VP pastes, where at 60 °C the concentrations were 276 mmol/L for 18VP-4L and 305 mmol/L for 25VP-10L. These are the highest Na concentrations of all investigated systems.

The concentration of K was highest for the PC pastes. Partial replacement of PC with limestone reduced the concentrations of K. Increasing the curing temperature did not have a large impact on the K concentration in the limestone pastes. Both FA and VP reduced the concentration of K more than limestone, indicating that the reaction of both FA and VP lead to higher uptake of K than release. Increasing the curing temperature did not have a large impact on the concentrations of K in any of the composite cement pastes.

The concentrations of S (primarily present as SO_4^{2-} in the solutions) consistently increase with increasing temperature, as reported previously [34,35]. This is attributed to the increased solubility of ettringite at higher temperature [35–38]. All composite cements have lower concentrations of S than PC, and the concentrations were lower at higher replacement level. This is likely due to the calcium sulphates in PC being the main sulphate source in the pastes. The reduced S concentrations in the composite pastes compared to the PC reference can possibly be related to the stabilization of ettringite over monosulphate in the presence of limestone [32].

The OH^- concentration calculated from charge balance (see Equation (1)) followed the same trends as the measured pH values, confirming that the pH and ICP measurements are consistent. Despite the Na and K concentrations being independent or increasing with the curing temperature, the OH^- concentration and thereby the pH decrease with increasing curing temperature. This is caused by the strong increase in the SO_4^{2-} concentration with increasing curing temperature.

The concentration of Al tended to decrease with increasing temperature. For PC-L, the concentrations were higher at 22 % than at 35 % replacement. PC-FA had lower or similar concentrations at 22 % and 35 % replacement, whereas the concentrations were similar for PC-VP at both replacement levels. The concentrations decreased in order PC-FA > PC-VP > PC > PC-L. The reduced concentration of Al with increasing temperature agrees with the literature [35,39].

The concentrations of Ca showed the same trend for all samples where 20 °C and 38 °C were similar, whereas 60 °C was higher. In order of increasing concentrations, the pastes were ranked PC-FA < PC-VP < PC-L ≤ PC.

There were no clearly defined trends for Si. One exception is the trend of decreasing concentration with increasing temperature for all samples except the PC-L pastes. The effect of replacement level was also inconsistent, with only minor differences. The overall concentration of Si increased in order from PC-L < PC < PC-VP < PC-FA.

3.3. Reaction of clinker and SCMs

The amounts of C_3S, C_2S, C_3A, C_4AF in each cement paste as determined by QXRD is summarised in Table 7 in "Appendix B: Quantitative X-ray diffraction. The amount of unreacted clinker was similar for all samples indicating a minor influence of the presence of SCMs on the clinker reaction after 180 days. Also, the temperature had no clear effect on the clinker reaction.

Fig. 6 shows the degree of reaction (DoR) of the SCMs obtained by mass balance. Note that one typically accounts for an error of roughly 10 % on the DoR of the SCMs [28]. Overall, the DoR of FA and VP in the

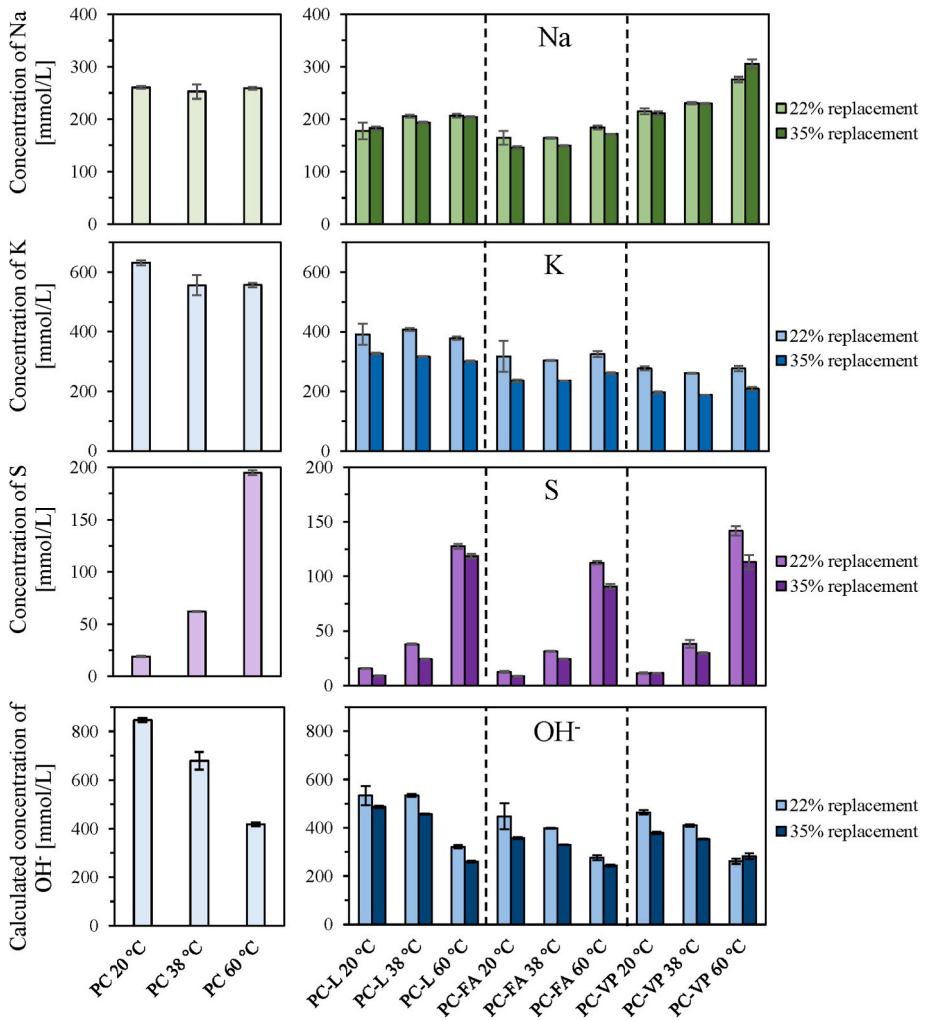

Fig. 4. Pore solution concentrations of Na, K, and S, together with a calculated OH^- concentration.

cement pastes are similar within the range of uncertainty. The DoR is similar for curing at 20 and 38 °C and ranges between 35 and 48 % for both SCMs, with a tendency of slightly higher DoR at lower replacement level and increasing curing temperature. Increasing the curing temperature to 60 °C had a considerable impact on the DoR, as it increases up to 74–77 % for 18FA-4L and 18VP-4L, and 52–54 % for 25FA-10L and 25VP-10L. The DoR for 22 % replacement at 60 °C is very high compared to the other samples and compared to the amount of reactive material in the SCMs. This might be an overestimation of the DoR resulting from the method that was used. These values should be verified with another method such as image analysis.

Fig. 7 shows the reacted and unreacted amounts of FA and VP in the cement pastes expressed relative to 100 g cement. The non-reactive part of FA and VP is the part which consists of minerals which are considered inert (see section 2.1). The reactive part of the SCM, i.e., sum of the reacted and unreacted part, is calculated by subtracting the non-reactive part from the total amount of SCMs in the system (Table 4). As a simplification, the reactive part is assumed to have a homogenous composition and to react congruently. This is known to be an over-simplification for e.g., fly ash containing systems [40]. Potential ways to improve our approach are discussed in the further research section (section 4.5.2). The typical 10 % error for the DoR of the SCMs [28] correlates to an error of about 2 g/100 g cement in Fig. 6.

In the mass balance the non-reactive part of the SCMs is independent of the curing temperature and increases slightly with increasing replacement level as the inert minerals are a fixed percentage of the SCM. It is about 3 g/100 g of cement for 18FA-4L and 18VP-4L, and about 4.3 g/100 g of cement for the 25FA-10L and 25VP-10L.

Of more interest are the variations in the reacted amount of the SCMs (Fig. 7). They are again quite similar for both SCMs investigated and are therefore discussed together. The impact of increasing the curing temperature from 20 to 38 °C is limited, the amount of reacted SCM lies between 7.6 and 11.0 g/100 g cement. There is a slight increasing trend in the amount of SCM reacted, i.e., about 1 g/100 g cement. Increasing the curing temperature to 60 °C leads to a considerable increase in the amount of reacted SCM, i.e., 13.0–13.9 g/100 g cement, which corresponds to an increase of about 4–5 g/100 g cement.

One of the main focuses of this paper is the impact of the replacement level on the alkali distribution in hydrated cement paste. From Fig. 7, we can see that increasing the SCM content from 18 to 25 wt%, only lead to a minor increase in the amount of SCM reacted. This means that the additional SCMs in the system, when increasing the SCM content, do not react and mainly function as filler. This is visualised in Fig. 7 by the increasing amount of unreacted SCM for the 25 % SCM blends compared the 18 % SCM cements.

3.4. Hydrate assemblage

TGA and XRD data indicate in all samples the formation of C-A-S-H, portlandite, ettringite, and AFm phases (monosulphate, monocarbonate, and hemicarbonate). Fig. 8 shows the CH and bound water content of the cement pastes hydrated for 180 days, normalized to 100 g dry

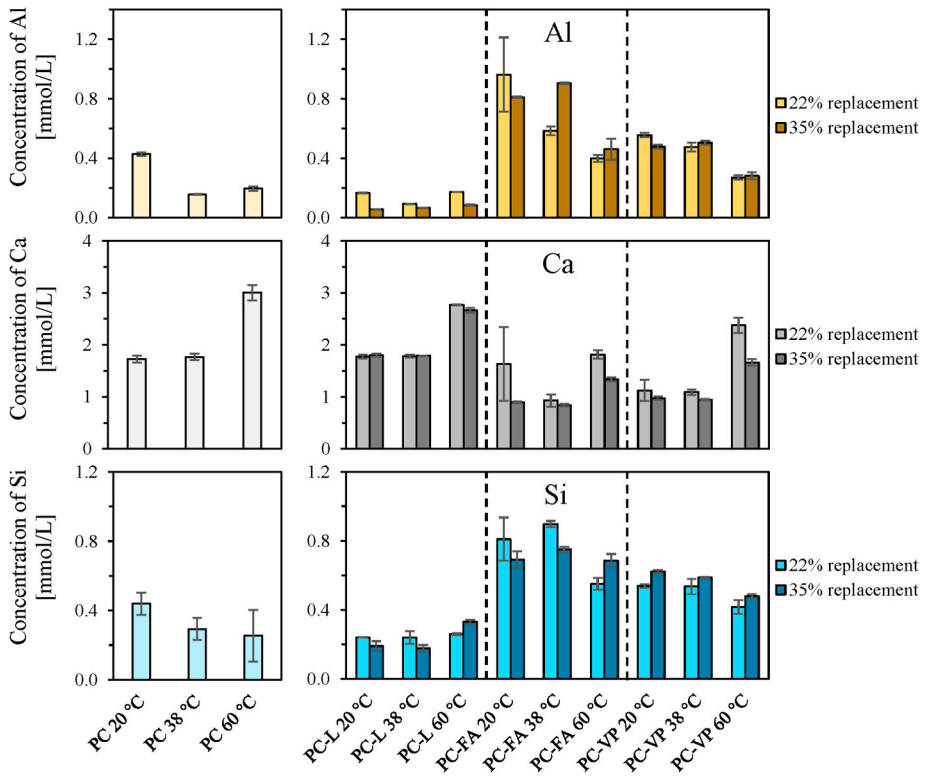

Fig. 5. Pore solution concentrations of Al, Ca, and Si.

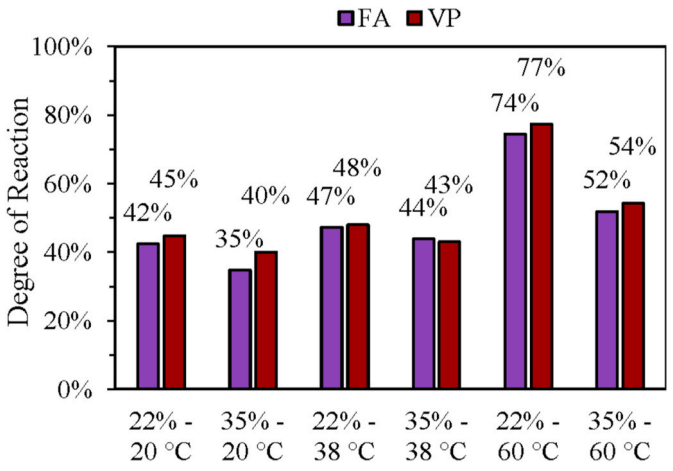

Fig. 6. Degree of reaction (DoR) of the FA and VP determined by mass balance. The pastes are organized by curing temperature and by replacement level (22 % and 35 %).

(composite) cement. Partial replacement of PC with limestone reduced the CH content. The portlandite content was further reduced in the presence of fly ash or volcanic pozzolan.

There was no clear effect of temperature on the amount of CH in the PC or limestone pastes, while all pastes with FA or VP showed decreasing CH contents with increasing temperature indicating increased pozzolanic reactivity.

Comparing the FA and VP pastes to the limestone pastes, there was a slightly larger reduction in CH content for the pastes with 35 % replacement than for those with 22 %. This suggests that there is slightly more reacted SCM in the pastes with 35 % FA and VP. The reduction in CH content was also larger for FA than VP by about 1 g/100 g cement. The difference between FA and VP also increased with increasing curing temperature. This is likely due to the higher Si-content in FA than in VP (see Table 1), which becomes more important as the replacement level and degree of SCM reaction increases.

The bound water content in all the pastes showed a small but consistent decreasing trend with increasing curing temperatures, agreeing with the literature [35,41–45]. There was also a small decrease in bound water with increased replacement level. The bound water content agreed with the values reported by Taylor [10]. Increasing the temperature led to similar reductions of bound water for the limestone pastes as for the PC pastes. This can be attributed to a lower degree of reaction of the clinker with increasing curing temperature, and/or to the formation of hydration phases containing less water [42,43]. At 20 °C the pastes with pozzolans had more bound water than the limestone pastes, but slightly less than the PC pastes. This indicates that the pozzolanic reaction led to the formation of more hydrates and thereby more bound water. Increasing the temperature caused similar reductions in bound water for all the pastes with SCMs. The pastes containing VP and FA cured at 60 °C typically have 4 g of bound water less compared to the same pastes cured at 20 °C, potentially due to the formation of less water-rich C-A-S-H at higher temperatures [34,41,42,44,46–48].

Table 7 in "Appendix B: Quantitative X-ray diffraction" shows the amount of ettringite, together with the amount of CH. The quantified amount of CH from QXRD is consistently lower than by TGA, likely due to parts of the CH being poorly crystalline or parts of the CH carbonating before analysis. A general trend of decreasing ettringite content with increasing temperature was observed, which was particularly notable at 60 °C. For all the pastes except PC there was also a trend of decreasing peak intensity of hemi- and monocarbonate whilst the amount of monosulphate increased from 20 to 60 °C.

3.4.1. C-A-S-H characterization with SEM-EDS

C-A-S-H is the main hydration phase and has a dominant influence on the mass balance calculations. The C-A-S-H composition of the different blends was characterised by SEM-EDS point scans and summarised in

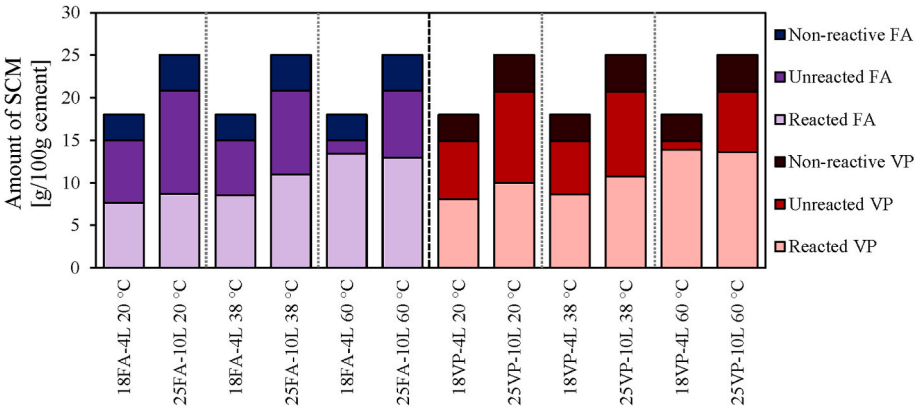

Fig. 7. Amounts of reacted and unreacted FA and VP in the composite cement pastes.

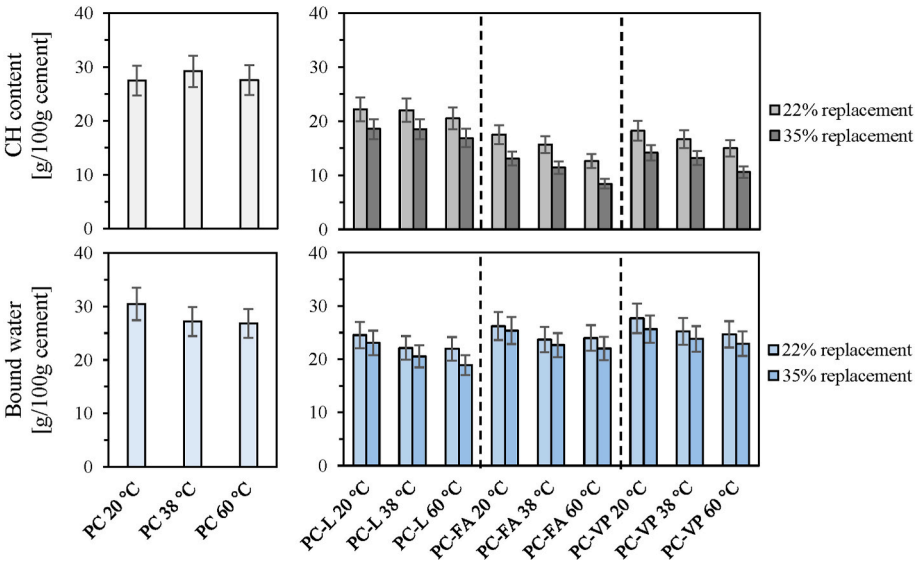

Fig. 8. CH content and bound water of the cement pastes hydrated for 180 days, normalized to 100 g dry (composite) cement. The uncertainty is estimated as 10 % of the absolute value.

Table 5. Detailed scatter plots for Al/Ca against Si/Ca are provided in "Appendix C: SEM-EDS." 100–300 point scans of inner product were used to determine the composition of C-A-S-H using atomic ratios, following a procedure similar to the graphical method described by Scrivener et al. [49]. This includes the Ca/Si, Al/Ca, Al/Si, and S/Si ratios. Fig. 9 shows the Al/Ca ratios of the cement pastes as they vary with the Ca/Si ratios.

One of the main challenges encountered with the SEM-EDS characterization of C-A-S-H in this study was the determination of the Ca/Si ratio. For the mass balance the 5th percentile of the Ca/Si ratio was used based on the traditional graphical scatter plot method described by Scrivener et al. [49]. The 5th percentile of Ca/Si corresponds to the 95th percentile for Si/Ca, which is typically where the traditional graphical interpretation of Al/Ca vs Si/Ca scatter plots end up selecting the Ca/Si for C-A-S-H. Similar reasoning was used to determine that the Al/Ca-ratio from the graphical interpretation was always very close to the median Al/Ca value, and the Al/Si ratio was equal to the 5th percentile of all Al/Si values. Fig. 10 uses 25FA-10L and 25VP-10L at 38 °C as examples to show how the 95th percentile Si/Ca, median Al/Ca and 5th percentile Al/Si almost intersect in a point, with only minor deviation. These lines should intersect at the same point, which corresponds to the composition of the C-A-S-H. In this work we chose to use the 95th percentile Si/Ca and median Al/Ca-ratios in the mass balance calculations, but the 5th percentile Al/Si-ratio could have been used with the same result.

According to TEM studies published by Richardson and co-workers [50–52] there should be a lower Ca/Si ratio limit around 1.3–1.4 whilst there is CH in the cement pastes, which is the case for all pastes in this study (Fig. 8). Using the graphical scatter plot method (or equivalently the 5th percentile of Ca/Si, see "Appendix C: SEM-EDS"), the resulting Ca/Si ratios for the samples with limestone, FA and VP are below 1.4. The results of the present study have been consistent, as multiple measurements of the same sample gave the same results. Using the Ca/Si ratios determined from these plots tended to underestimate the Ca/Si in the cements, resulting in too much portlandite in the mass balance. This, combined with the publications of Richardson [50,51,53], were the reasons we used the 5th percentile combined with a lower limit of 1.4 for Ca/Si.

There are a few possible explanations for the low Ca/Si ratios measured by SEM-EDS. For the pastes containing FA and VP there could be fine intermixing of silica rich SCM particles in the measured points. The composite pastes show a large spread in measured Si/Ca values compared to the PC pastes (see "Appendix C: SEM-EDS"), which could suggest that the measured points are C-A-S-H intermixed with the siliceous SCMs. This would result in a shift towards the composition of FA or VP, both in terms of Si/Ca and Al/Ca. Fig. 10 examines this hypothesis, using 25FA-10L and 25VP-10L at 38 °C as examples. If a large part of the SEM-EDS point scans had intermixed FA or VP, we should expect

Table 5
Summary of atomic ratios from SEM-EDS point scans of the cement pastes, organized by replacement type and with alternating 22 % and 35 % replacement level. The numbers are based on 100–300 point scans of inner product. 5th percentile Ca/Si-values marked with (*) were deemed below reasonable values, and in these cases Ca/Si 1.4 was used for the mass balance calculations. Median Ca/Si is also included for the purpose of method discussion. Median Ca/Si, Al/Si, Na/Si and K/Si were not used as input for the mass balance and are therefore in italic font.

Cement	Curing temperature [°C]	Ca/Si (5th perc.) [−]	*Ca/Si (median)* [−]	Al/Ca [−]	S/Si [−]	*Al/Si* [−]	*Na/Si* [−]	*K/Si* [−]
PC	20	1.81	*2.04*	0.07	0.12	*0.10*	*0.024*	*0.019*
	38	1.61	*1.76*	0.05	0.10	*0.07*	*0.021*	*0.014*
	60	1.65	*1.83*	0.04	0.09	*0.05*	*0.017*	*0.011*
22L	20	1.68	*1.97*	0.06	0.10	*0.06*	*0.039*	*0.042*
35L	20	1.35*	*1.58*	0.06	0.06	*0.05*	*0.048*	*0.033*
22L	38	1.67	*1.83*	0.05	0.07	*0.07*	*0.031*	*0.031*
35L	38	1.19*	*1.46*	0.06	0.05	*0.07*	*0.036*	*0.019*
22L	60	1.31*	*1.53*	0.06	0.06	*0.06*	*0.023*	*0.008*
35L	60	1.34*	*1.53*	0.07	0.04	*0.08*	*0.020*	*0.000*
18FA-4L	20	1.46	*1.67*	0.10	0.06	*0.12*	*0.020*	*0.027*
25FA-10L	20	0.94*	*1.37*	0.14	0.05	*0.12*	*0.067*	*0.058*
18FA-4L	38	1.49	*1.66*	0.09	0.07	*0.12*	*0.017*	*0.026*
25FA-10L	38	0.99*	*1.27*	0.17	0.05	*0.15*	*0.070*	*0.073*
18FA-4L	60	1.00*	*1.26*	0.14	0.05	*0.13*	*0.106*	*0.106*
25FA-10L	60	1.02*	*1.38*	0.15	0.05	*0.15*	*0.054*	*0.074*
18VP-4L	20	1.43	*1.66*	0.08	0.07	*0.10*	*0.016*	*0.010*
25VP-10L	20	0.79*	*1.09*	0.13	0.03	*0.10*	*0.102*	*0.047*
18VP-4L	38	1.46	*1.71*	0.08	0.07	*0.10*	*0.015*	*0.010*
25VP-10L	38	0.86*	*1.22*	0.13	0.04	*0.11*	*0.099*	*0.048*
18VP-4L	60	0.93*	*1.24*	0.12	0.05	*0.10*	*0.116*	*0.043*
25VP-10L	60	0.86*	*1.22*	0.13	0.04	*0.11*	*0.099*	*0.048*

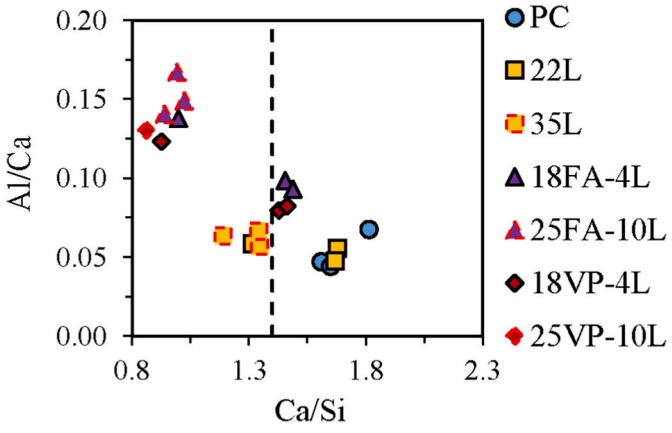

Fig. 9. Summary of Al/Ca and Ca/Si values for C-A-S-H in the cement pastes as determined by SEM-EDS. The Al/Ca values were used for the mass balance, whereas a lower limit of 1.4 was enforced for the Ca/Si ratios (shown as a dashed black line).

to see points trending from the "centre of mass" of the point cloud towards the Al/Ca and Si/Ca-ratio of the unreacted SCMs. Fig. 10 illustrates this by drawing lines from where most points are located, then upwards with a slope equal to the Al/Si ratio of unreacted FA and VP. We can see that there are only a handful of points that trend in this direction, even fewer than the points that trend towards AFm (Al/Ca = 0.5, Si/Ca = 0). The majority of points for the IP instead follow an Al/Si ratio trending from the origin, with a slope near the 5th percentile Al/Si of all measured IP points. The 5th percentile corresponds to the "lower bound" of the scatter plot, which represents the Al/Si ratio of the C-A-S-H. This suggests that for most measurements, each point is mainly a mixture of C-A-S-H and varying amounts of CH, AFm, and potentially C_4AF, whilst the intermixing of unreacted FA and VP is limited.

In cases such as 25FA-10L in Fig. 10 it appears as though using the rightmost edge of the point cloud as suggested by Scrivener et al. [49] does not give a good representation of the Ca/Si ratio in the C-A-S-H. For this paste the outer edge would give a Ca/Si ratio of 0.8. We could instead investigate what ratios arise from using the median Ca/Si value. Comparing the 5th percentile (outer edge) to median Ca/Si in Table 5, we see that using the median Ca/Si naturally increases Ca/Si for all pastes. The highest value becomes 2.04 for PC at 20 °C. On the other extreme, 25VP-10L increases from the 5th percentile of 0.79 to median of 1.09, much closer to a reasonable value. All these values below 1.4 would still cause major issues for the mass balance, so there is still a

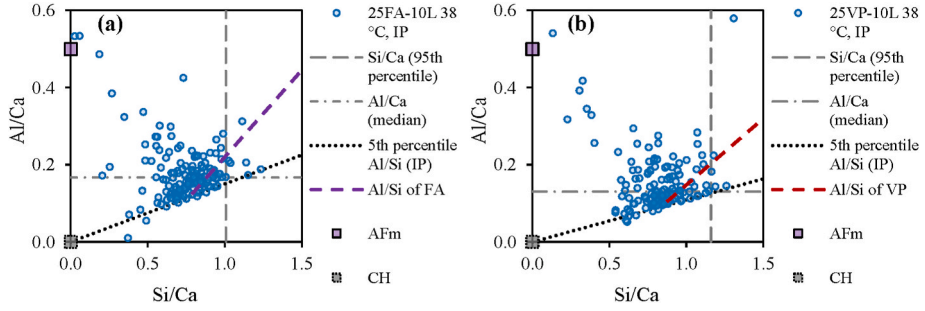

Fig. 10. Al/Ca against Si/Ca scatter plot for the inner product (IP) in the 25FA-10L (a) and 25VP-10L (b) cement pastes cured at 38 °C. Also plotted in the figures are the 5th percentile Al/Si values, 95th percentile Si/Ca values (reciprocal of 5th percentile Ca/Si), and median Al/Ca for these points, together with the Al/Si ratio of unreacted FA and VP. The compositions of AFm and CH are included to show how the points from SEM-EDS arrange in the "triangle" between AFm, CH, and C-A-S-H. The Al/Si ratios of the unreacted SCMs start in the centre of the point clouds to illustrate where points of IP intermixed with unreacted SCM would trend towards.

disconnect between the C-A-S-H characterization and the chemistry of the paste overall.

3.4.2. Variations in C-A-S-H composition determined with SEM-EDS

The binder and curing temperature also impact the C-A-S-H composition, as visible in the median values for the Al/Ca, S/Si, Na/Si and K/Si ratio, and the 5th percentile for the Ca/Si ratio (Table 5). Fig. 9 shows the Al/Ca (median) and Ca/Si (5th percentile) ratios for C-A-S-H in the investigated cement pastes.

For PC, increasing the curing temperature resulted in a reduction of the Ca/Si ratio from 1.81 at 20 °C to 1.65 at 60 °C. The Al/Ca ratio decreased from 0.07 to 0.04, S/Si from 0.12 to 0.09, Na/Si from 0.024 to 0.017 and K/Si from 0.019 to 0.011.

At 20 °C, partial replacement with limestone reduced the Ca/Si, Al/Ca, and S/Si ratios. The reduction was larger for 35L than 22L, except for Al/Ca which was similar for both replacement levels. The K/Si and Na/Si ratios increased with limestone replacement. The increase in Na/Si was larger for 35L than 22L, whereas for K/Si the increase was larger for 22L. Especially notable is that the replacement of PC with limestone resulted in a considerable reduction of the Ca/Si ratio: Ca/Si ratio for 22L was 1.68, and for 35L it was 1.35.

Replacing PC with FA at 20 °C reduced the Ca/Si further than pure limestone replacement. The Al/Ca ratio was increased compared to PC-L. Na/Si and K/Si were lower for 18FA-4L than 22L, but higher for 25FA-10L than 35L. Increasing the curing temperature to 60 °C reduced the Ca/Si ratio of 18FA-4L, but there was little effect on 25FA-10L. The Na/Si ratio in 18FA-4L was similar at 20 and 38 °C but spiked at 60 °C. 25FA-10L had similar Na/Si ratios at 20 and 38 °C but showed a decreasing ratio at 60 °C. K/Si showed the same trend as Na/Si for 18FA-4L, only increasing from 38 to 60 °C. For 25FA-10L the K/Si ratio increased from 20 to 38 °C but did not change much at 60 °C.

Replacement of PC with VP had similar effects as FA at 20 °C. The Ca/Si ratio decreased, whilst the Al/Ca ratios were higher than with limestone but lower than with FA. The Na/Si and K/Si ratios were much higher at 35 % than at 22 % replacement. Increasing curing temperature reduced the Ca/Si ratio for 18VP-4L. The Al/Ca ratio increased for 18VP-4L at 60 °C but did not change much for 25VP-10L. 18FVP-4L had similar Na/Si at 20 and 38 °C but as for 18FA-4L it spiked at 60 °C. 25VP-10L had little effect of temperature on the Na/Si ratio. For K/Si, both VP pastes showed similar trends as for Na.

3.4.3. Amount of C-A-S-H

Fig. 11 shows the amount of C-A-S-H calculated by mass balance in the investigated systems. It is divided in the amount of SiO_2, Al_2O_3, CaO and H_2O, to illustrate the variation in composition amongst the different systems. The pozzolanic SCMs contribute mainly with Si and Al to the C-A-S-H composition. The figure shows that replacing PC with limestone causes a decrease in C-A-S-H content.

When parts of PC are replaced with both pozzolana and limestone, there is more C-A-S-H than in the case of limestone only and a stronger temperature dependency of the amount of C-A-S-H due to the variation of the degree of reaction of the pozzolans with temperature (Fig. 6). The amount of C-A-S-H is higher in PC-FA and PC-VP than in PC-L due to the pozzolanic reaction. However, the final amount of C-A-S-H is slightly lower than the pure PC pastes except at 60 °C. Although the total mass of C-A-S-H is lower at higher replacement levels, the mass of (Si + Al) in the FA pastes are both higher than PC. The PC-VP pastes show similar trends, with around 10 % less total C-A-S-H than the pastes with FA across both replacement levels and all temperatures. This is true both in terms of total mass of C-A-S-H, and in terms of (Si + Al).

3.4.4. Summary of hydrates based on mass balance

Fig. 12 shows the phase distribution of the hydrated cement pastes as calculated by mass balance based on the cement composition and the amount of unreacted clinker and SCM as detailed in section 3.2. The mass balance calculations indicate that C-A-S-H and portlandite make up most of the hydrate assemblage in all the pastes. The amounts of other hydrates (ettringite, AFm phases, hydrotalcite and hydrogarnet) corresponds to roughly 10 wt% of the hydrated cement. Alkali metals are associated either with the non-reactive and unreacted part of the SCMs and PC, with C-A-S-H, or with the pore solution. The mass balance also captures the behaviour of increasing temperature destabilizing the

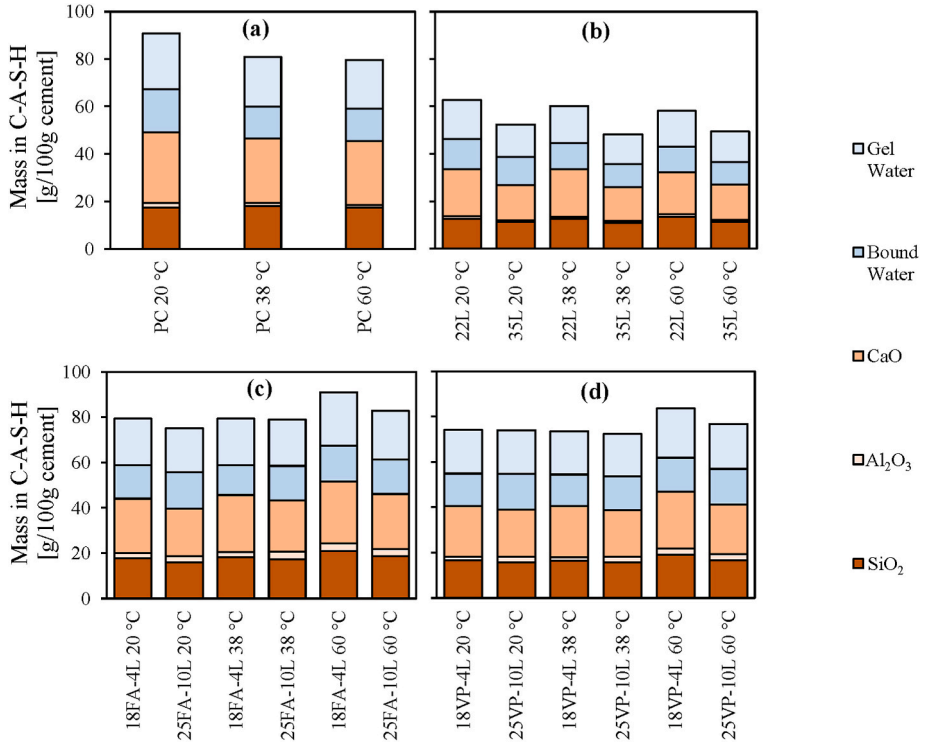

Fig. 11. Amounts of SiO_2, Al_2O_3, CaO, and water incorporated in C-A-S-H for the different cement pastes: (a) PC, (b) PC-L, (c) PC-FA, and (d) PC-VP.

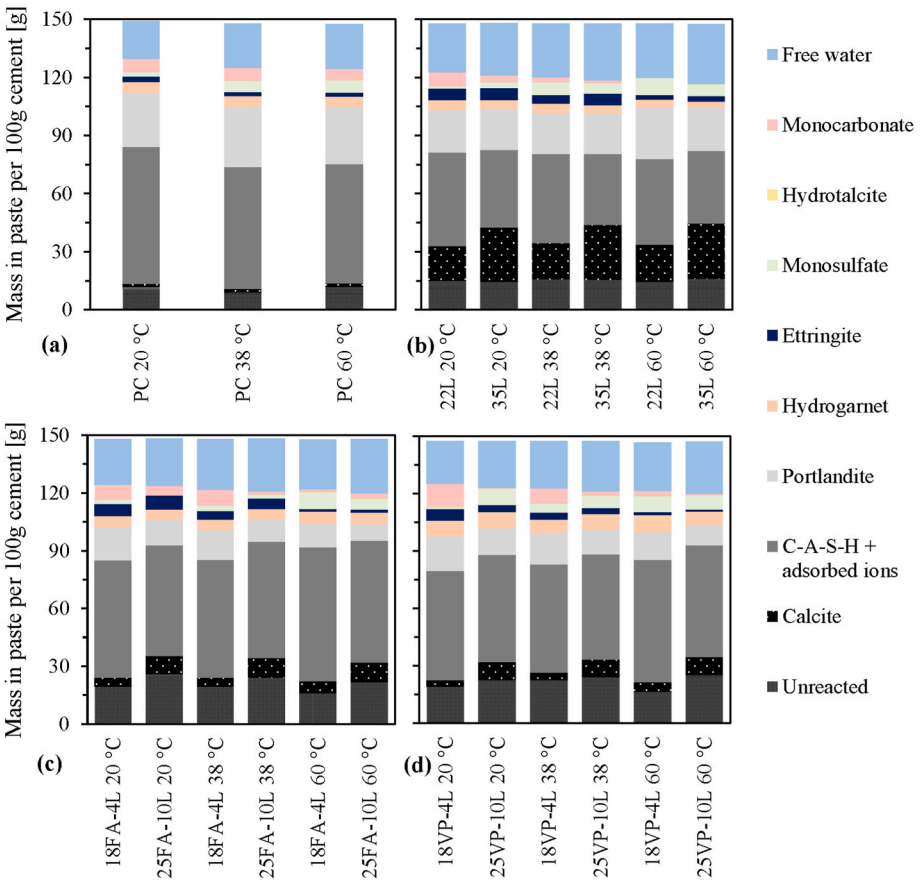

Fig. 12. Phase distribution of the cement pastes hydrated for 180 days as calculated via the mass balance.

ettringite-monocarbonate AFm system to instead prefer monosulphate AFm [35,36]. We have explored this further in a follow-up study.

3.4.5. Comparison of alkali uptake by C-A-S-H based on mass balance and SEM/EDS

Fig. 13 shows a comparison between the Na/Si and K/Si-ratios calculated from the mass balance (based on the XRF data, the degree of reaction, the amount of alkali in the pore solution and in unreacted clinker and SCMs), and the values determined by SEM-EDS (Table 5). There is generally a poor agreement between these two sets of results, where the SEM-EDS have much higher maximum values and lower minimum values.

According to the mass balance (based on the XRF data and the measured degree of reaction) there is little to no effect on Na/Si and K/Si with increasing replacement level of limestone, FA, or VP (Fig. 13). The Na/Si ratio for the investigated systems varies between 0.02 and 0.03. The K/Si ratio is around 0.03 for the PC and L system, and between 0.03 and 0.05 for the VP and FA containing systems, showing that there is a slight increase when pozzolans are included. The mass balance predicts similar Na/Si ratios as the ones measured by SEM-EDS for the PC systems, but besides this there is little correlation to the SEM-EDS results.

In contrast, according to SEM-EDS, limestone replacement increases both the Na/Si (0.02–0.05) and K/Si (0.01–0.04) ratios of the C-A-S-H compared to Na/Si (0.01–0.02) and K/Si (0.01–0.02) of the reference PC. The ratios varied with replacement level, where the Na/Si went slightly up and the K/Si slightly down with increasing replacement level. For both the PC and limestone references the Na/Si and K/Si decreased with increasing curing temperature, in contrast to the mass balance calculations. The 18FA-4L and 18VP-4L pastes have Na/Si and K/Si ratios in the range of the PC reference, except for the ones cured at 60 °C which are about 5 times higher. This is potentially due to the exceptionally high DoR of the SCM for these mixes at 60 °C (Fig. 6) and/or to a preferential dissolution of alkalis from the non-reactive fraction at high temperatures. 25FA-10L and 25VP-10L showed considerably higher Na/Si and K/Si ratio compared to 18FA-4L and 18VP-4L, ranging from double to 5 times higher. The pastes with FA showed the highest K/Si ratios, increasing from 0.05 to 0.08 with increasing temperature. For the VP pastes the K/Si is slightly lower than for FA and remains constant about 0.06 independent of the curing temperature. The higher K uptake in the C-A-S-H for the FA containing mixes compared to the VP blends relates to the relatively high reactive K content in FA. The Na/Si ratio of the 35 % replacement level FA systems was about 0.05, and for the equivalent VP systems the Na/Si ratio increased to 0.10–0.13, likely because of VP contributing with additional Na to the system. We can conclude from this that although the composite cement pastes with 22 % replacement have more C-A-S-H than at 35 % replacement at 20 and 38 °C, the C-A-S-H at 35 % replacement seems to bind considerably more Na and K per molar unit according to the SEM-EDS measurements.

Solving the disagreement between mass balance and SEM-EDS is very important to understand the distribution of alkali metals in cement paste and concrete. The issue can be approached from either side to hopefully determine which method most closely represents reality. Assuming that the mass balance (or rather the XRF measurement of alkali content and the assumption of homogeneous dissolution) is most incorrect, we can evaluate which inputs and assumptions could be changed to make the output closer to the experimental data from SEM-EDS. It is possible:

i) that the total alkali metal content obtained from XRF is too low, as it has been documented that XRF underestimates Na and K content compared to dissolution experiments [29], which would

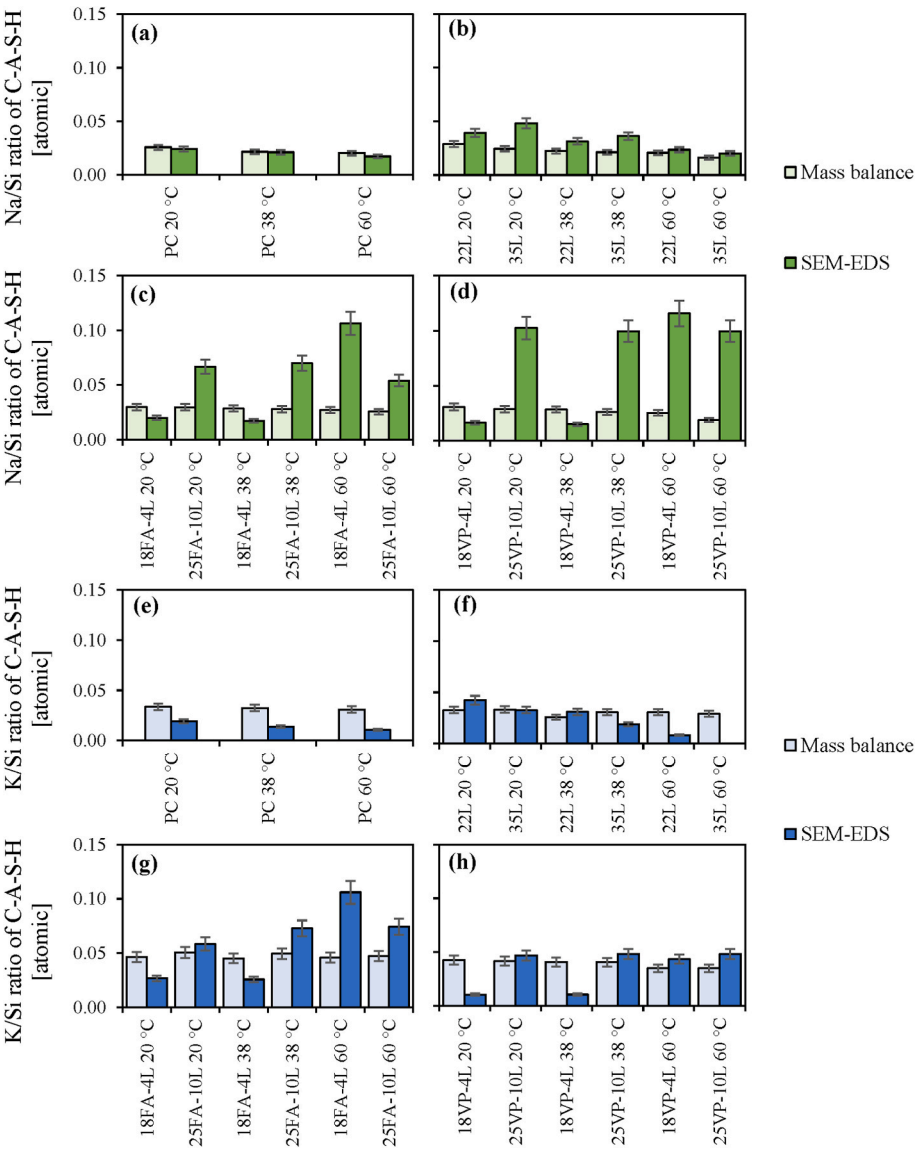

Fig. 13. Comparison of Na/Si (a–d) and K/Si (e–f) for the cement pastes, as calculated with the mass balance or as the median values from SEM-EDS point scans of inner product. The black bars represent an estimate of 10 % error in the measurements.

lead to an underestimation of the Na/Si and K/Si based on mass balance.

ii) For the composite cements, and especially those with VP, the assumption that most Na- and K-bearing minerals are unreactive could be wrong, which would lead to an underestimation of Na/Si and K/Si in particular for the blended cements.

iii) It could also be the case that the amorphous phases dissolve incongruently, thereby also releasing more Na or K than Si (as used in previous models [10,17]). These ideas could be verified experimentally by using SEM-EDS with mineral identification and focusing on these unreacted phases to see if their compositions and degree of reaction change over time. However, even if it was assumed that all Na and K would be released, the resulting Na/Si ratios are still lower than those measured with SEM-EDS (see supplementary data).

iv) Alternatively, the amount of C-A-S-H and the amount of Si in it could be overestimated or the degree of FA and/or PV reaction. To get the same Na/Si and K/Si ratios from SEM-EDS as with the mass balance would require both more Na or K released into the system and less Si in C-A-S-H.

There are also potential issues with the SEM-EDS characterization of C-A-S-H. Sample preparation is one of the major sources of uncertainty [17]. It is difficult to know what cutting, storing in isopropanol, and then polishing the sample does to the final surface that is scanned. The preparation could leach out alkali metals which would reduce the Na and K content. Simultaneously there could be precipitation of alkali hydroxides or other phases that would enrich the surface content. At 60 °C there could even be the formation of alkali metal bearing phases similar to ASR products [54] which are not accounted for in the mass balance calculations. However, if precipitation was the cause we should expect to see more precipitation for the PC pastes as they had higher concentrations of Na and K than most of the FA and VP pastes, the key exceptions being the VP pastes at 60 °C.

There is also the chance that parts of the pore solution rich in Na and K are still present in the smallest pores of the paste [55], which means that rather than scanning points of C-A-S-H we are scanning points of C-A-S-H and pore solution. This would contribute to increased alkali metal contents, beyond the actual adsorption in C-A-S-H. All of these issues appear before interaction with the SEM. During the SEM-EDS analysis the alkali metals can be evaporated by the beam [49], and the mass percent of Na and K can sometimes be below the detection

limit. Manual point selection is also susceptible to user bias.

In summary, both methods are associated with errors and uncertainties and the real values might lie somewhere between the two methods.

3.5. Alkali metal distribution

3.5.1. Alkalis in unreacted and non-reactive phases

The variations in the amounts of reacted and unreacted SCM translate in variations of their alkali metal contributions to the system. Figs. 14 and 15 shows the calculated distribution (based on the XRF composition) of the alkali metals in the non-reactive and unreacted parts of the cement pastes, including PC, limestone, and the SCMs. The non-reactive part of the alkali metals in the SCMs is the part which is locked in the inert minerals (see section 2.1). For FA none of the non-reactive minerals contain alkali metals, whereas around 40 wt% of the Na in VP was locked in minerals like andesine (Table 3).

From Fig. 14 we can see that only a minor share of the total alkali metal content is found in unreacted clinker. Limestone contains non-reactive mineral phases, which host a considerable part of K and minor amounts of Na. In the case of VP, a large part of the Na is in non-reactive mineral phases and a considerable share is in the unreacted amorphous fraction. K is not retained in non-reactive part of VP, and only very little is in the unreacted share. For FA both Na and K can be found in the unreacted share, with slightly more K than Na due to the composition of the FA. These calculations are based on the composition determined by XRF, which potentially underestimates the alkali content present in the cement [29].

3.5.2. Alkali metal distribution in hydrated cements

Figs. 16 and 17 show how Na and K are distributed between pore solution, C-A-S-H, unreacted phases, and non-reactive phases in the cement pastes as determined by the mass balance. Fig. 16 gives the distribution in absolute terms with mmol/100 g (composite) cement, whereas Fig. 17 gives the values as percentages of the total Na and K content. The amount of alkali metals in the pore solution was calculated as the product of the concentrations measured with ICP (Fig. 4 and Table 6) and the volume of free water measured with TGA (Fig. 8).

Unreacted phases cover both unreacted clinker minerals and unreacted parts of the reactive SCM fraction (see Figs. 7 and 14). The amounts of clinker minerals was determined by using QXRD, and then multiplying these amounts with a wt.% of Na and K based on the clinker mineral composition table from Taylor [31] (Fig. 14). Amounts of non-reactive Na and K in the limestone and SCMs were also determined using the amounts of non-reactive, alkali metal bearing minerals from QXRD of the raw materials (Fig. 14). Subtracting non-reactive, unreacted, and pore solution from the total results in the Na and K adsorbed on C-A-S-H.

4. Discussion

4.1. How does increasing the replacement level of PC with SCMs affect the pore solution and concrete expansion?

Fig. 18 shows the expansion of the concrete prisms in the present study, plotted against the sum of Na and K concentrations in the cement paste pore solutions after curing for 90 and 180 days. Some studies have shown that there appears to be an alkali metal concentration in the pore solution below which concrete does not expand. Duchesne and Bérubé [18] found a lower limit of 650 mmol/L (Na + K) for long term expansion of concretes with two reactive aggregates (siliceous limestone and rhyolitic tuff), and Portland composite cements containing silica fume, fly ash or blast furnace slag. Bleszynski [56] reported a lower hydroxyl concentration limit for expansion around 320–360 mmol/L for concrete blends with binary and tertiary blends of silica fume and slag with reactive Spratt aggregate. At lower curing temperatures (20 and 38 °C) the hydroxyl concentration can be assumed to be nearly equal to the concentration of (Na + K) [10]. Bagheri et al. [5] observed that for a Swiss Uri aggregate with a range of binders, there was a lower limit of 300 mmol/L (Na + K). Tapas et al. [57] reported expansion and pore solution composition for concrete made with rhyolite and dacite aggregates, where a lower limit of expansion appeared around 400 mmol/L (Na + K) at 168 days.

Our findings agree with these studies, with the concentration limit of (Na + K) being around 450 mmol/L at 38 °C and 60 °C for our blend of reactive aggregates. The PC paste has naturally the highest concentration of (Na + K), above 800 mmol/L and showed considerable expansion. Partial limestone replacement did reduce the alkali concentration

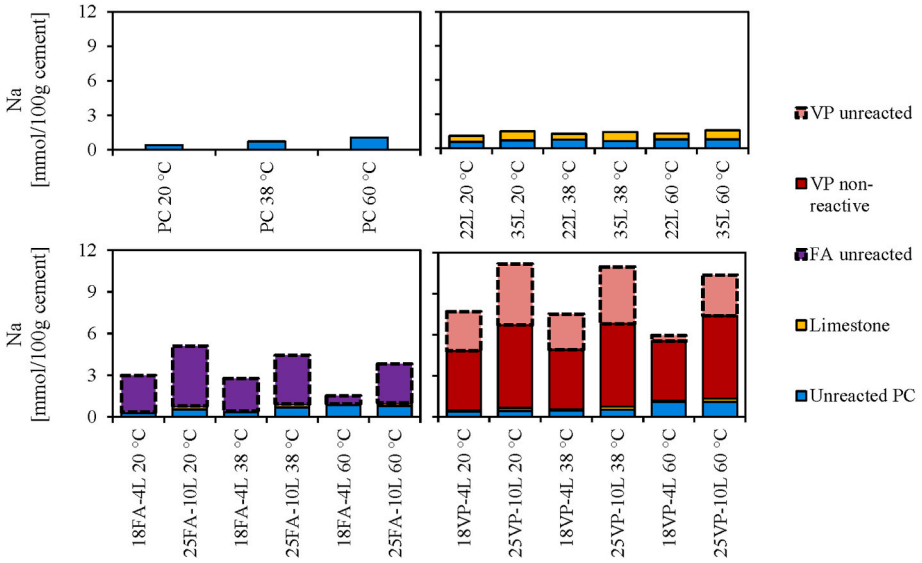

Fig. 14. Distribution of Na in the non-reactive and unreacted parts of the PC, L and SCMs in the mass balance.

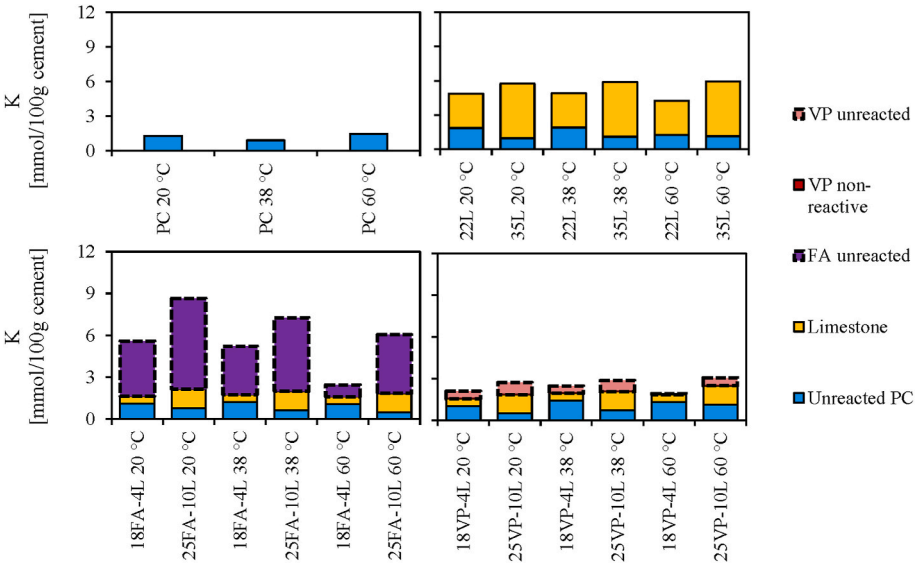

Fig. 15. Distribution of K in the non-reactive and unreacted parts of the PC, L and SCMs in the mass balance.

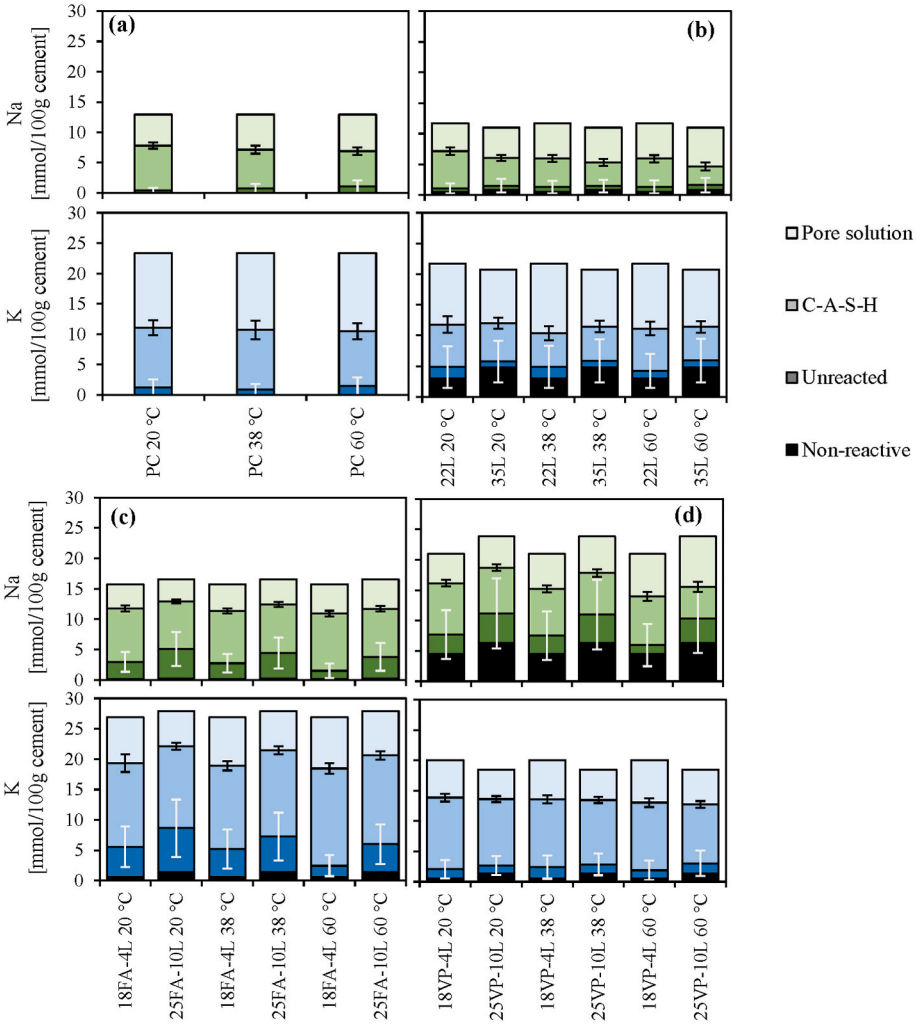

Fig. 16. Alkali metal distribution in the cement pastes, given as total amount of Na and K per 100 g (composite) cement. (a) is the PC pastes, (b) is PC-L, (c) is PC-FA, and (d) is PC-VP. The black error bars are the uncertainty in the amount of Na and K in the pore solution, whereas the light grey bars are the uncertainty in the amount of Na and K in unreacted and non-reactive phases combined.

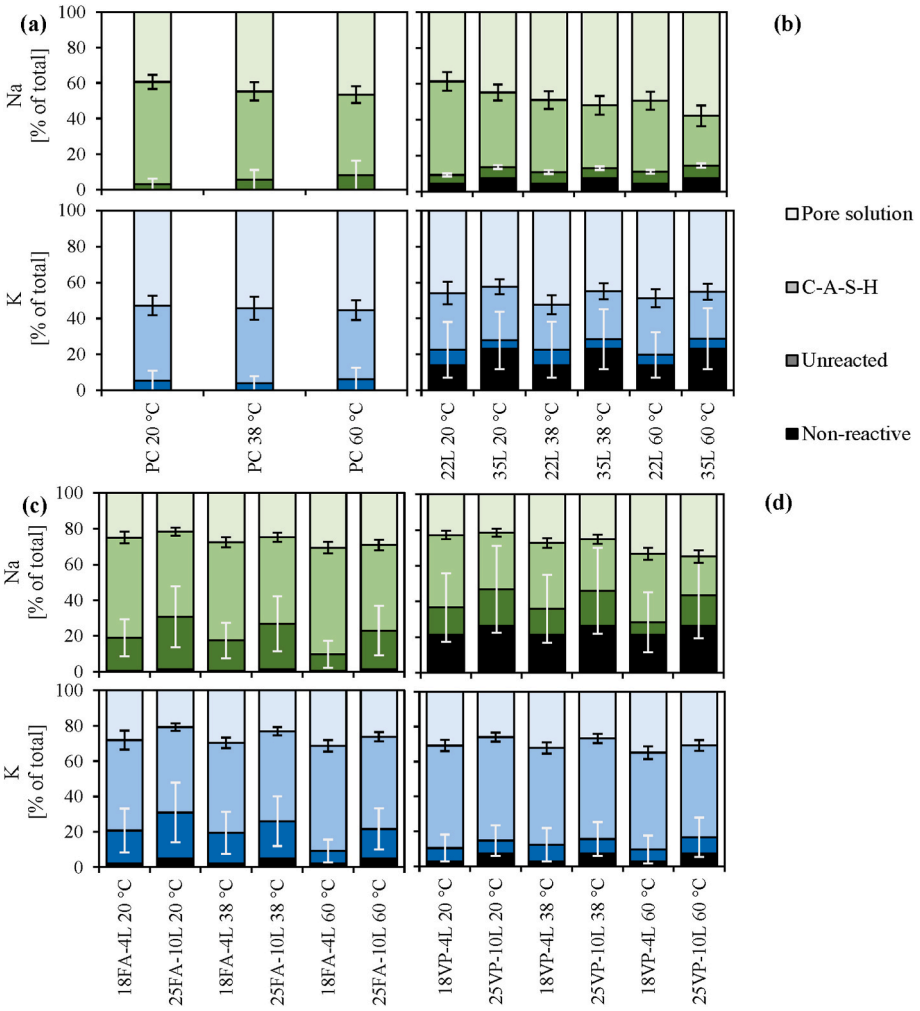

Fig. 17. Alkali metal distribution in the cement pastes, given as percentages of total Na and K content in each (composite) cement paste. (a) is the PC pastes, (b) is PC-L, (c) is PC-FA, and (d) is PC-VP. The black error bars are the uncertainty in the amount of Na and K in the pore solution, whereas the light grey bars are the uncertainty in the combined amount of Na and K in unreacted phases.

and the expansion. More limestone led to larger reduction in alkali concentrations, but the reduction was only proportional to the replacement level. To reach the lower concentration limit of 450 mmol/L with only limestone, around 50 % or more PC would have to be replaced, which is unrealistic as it would impair other properties of the concrete such its mechanical strength, permeability, and frost resistance.

In contrast to limestone, the pozzolanic SCMs are able to reduce the concentration of (Na + K) more efficiently, and thereby prevent expansion. This is despite the increased alkali metal content of both SCMs compared to the PC, where FA has a high content of K and VP has a high content of Na (see Table 1). The 18FA-4L pastes had (Na + K) concentrations around 470–500 mmol/L and showed slight expansion. Increasing the replacement level of FA, 25FA-10L decreased the (Na + K) concentration to 380–430 mmol/L, and this was sufficient to prevent expansion. The story for VP was similar at 20 and 38 °C. 18VP-4L had around 490 mmol/L (Na + K), and 25VP-10L had 410–420 mmol/L. However, at 60 °C there was a spike in Na concentration in the VP pastes, resulting in (Na + K) concentrations of 550 mmol/L for 18VP-4L and 515 mmol/L for 25VP-10L. Although concrete prisms for 25VP-10L and 25FA-10L at 60 °C are missing, we could expect based on the (Na + K) concentrations that 25VP-10L would likely expand.

Such a maximum limit for the sum of Na and K concentrations in the pore solution could be a good measure to target when designing concrete mixes that can resist ASR. It is most likely that the exact value for this limit is dependent on the type of aggregates, but our findings suggest it might be independent of curing temperature. The concept of a lower alkali metal concentration limit partially answers why pozzolanic SCMs can mitigate ASR, as they are effective at reducing the concentration of (Na + K) in the pore solution. Higher replacement levels lead to lower alkali metal concentrations, except in the case of Na in the VP pastes. The questions that remain are by what mechanisms do the pozzolans reduce the alkali metal concentrations, and how does the replacement level of SCM influence these mechanisms.

4.2. How does increasing the replacement level of PC with SCMs affect the alkali metal distribution in the solids?

Replacing PC with SCMs can lead to an increase in the total amount of alkali metals in the system compared to the reference PC system, which does not necessarily translate into more reactive alkali metals. From Fig. 16 we can see that the FA containing composite cements have a 25–35 % higher total Na and about 20 % higher K content than PC. The VP cements have a 70–90 % higher Na content, but a 10–20 % lower total K content compared to PC. However, a considerable part of these alkali metals is present in non-reactive and unreacted phases (Figs. 16 and 14).

Fig. 19 shows the "reactive" alkali metals in the investigated cement pastes, meaning that we subtracted the unreacted and non-reactive shares (Fig. 14) from the total (Fig. 16). There are generally only

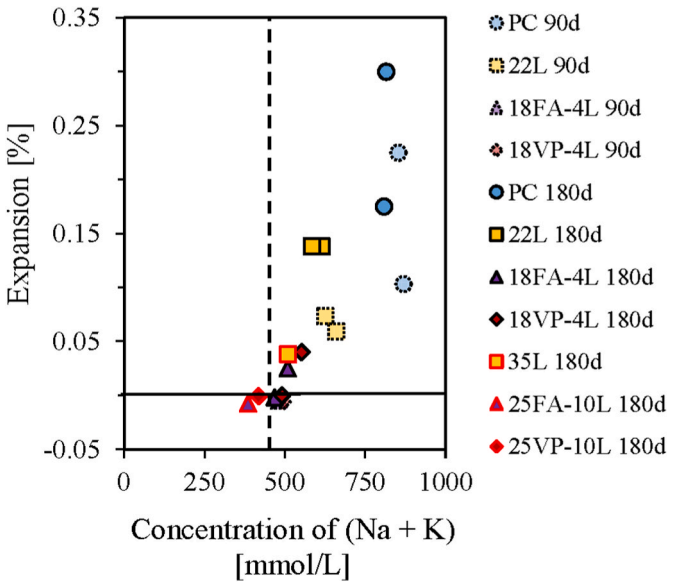

Fig. 18. Expansion of concrete prisms cured at 38 °C or 60 °C for 90 or 180 days as a function of the sum of Na and K concentrations in the cement paste pore solutions at the respective temperature after 180 days. A dashed line is included to show the concentration below which there is no expansion.

small differences between the amount of Na in pore solution at 22 % and 35 % replacement level, whereas the amount in C-A-S-H is lower at 35 % than 22 %. Limestone replacement reduced the reactive Na content. The reactive Na content in the pastes with FA and VP is fairly similar to the PC reference, with a slight shift towards less Na in pore solution and more in C-A-S-H. Elevating the temperature increased the DoR of the SCMs, thereby also increasing the amount of reactive Na.

For K there was a trend of less K being in the pore solution with increasing replacement level, which was not observed for Na. Most of this difference is accounted for by the lower amount of K in the pore solution. The amount of reacted K in the pastes is reduced by increasing the replacement level, because more K is retained in unreacted phases as more of the SCM remains unreacted (Fig. 7).

The pastes containing FA and VP systems have a similar or slightly lower reactive alkali metal load compared to the reference PC system. Increasing the replacement level seemed to cause a small decrease in the reactive alkali metal content, but the replacement level only decreased the amount of K in solution, not the amount of Na. The answer as to why the SCM containing systems have lower alkali metal concentrations in the pore solution compared to the PC reference, is not to be found in the difference in reactive alkali metal content. This rather lies in the change the distribution between the pore solution and the C-A-S-H as illustrated in Fig. 19. Thus, to understand the impact of the replacement level of the SCMs on the alkali metal concentration in the pore solution, we need to understand how they alter the C-A-S-H.

4.3. How does increasing the replacement level of PC with SCMs affect alkali metal binding by C-A-S-H?

To understand how pozzolans like FA and VP lower the alkali metal concentration in the pore solution, we need to understand how they affect the alkali metal uptake in C-A-S-H. The alkali metal content in C-A-S-H is determined by the amount of C-A-S-H, and the chemical properties of the C-A-S-H in terms of atomic ratios.

4.3.1. Amount of C-A-S-H

Fig. 11 gives the amounts of C-A-S-H for all the cement pastes. Replacing PC with limestone resulted in decreased mass of C-A-S-H, and the decrease was larger at 35 % than at 22 % replacement, as expected. The pastes with SCMs had more C-A-S-H than the limestone pastes, but less than the pure PC pastes. The only exceptions were 25FA-10L and 25FA-10L cured at 60 °C which had a similar amount of C-A-S-H as the PC reference. Similarly, as for the limestone pastes, the PC-FA and PC-VP pastes formed less C-A-S-H at higher replacement level.

The fact that increasing the replacement level by adding more FA and VP does not increase the total mass of C-A-S-H can be related to the amount of SCM that reacts. Fig. 7 shows that at the same temperature, similar amounts of SCM react for both 22 and 35 % replacement. This means that the additional SCM added acts merely as a filler and does not significantly contribute to forming more C-A-S-H after curing for 180 days. We can conclude that the ASR mitigating properties of FA and VP are not caused by the formation of more C-A-S-H than in PC pastes, which means the cause must lie in the chemical and physical properties of the C-A-S-H that forms.

4.3.2. Alkali metal uptake in C-A-S-H

We will now consider the changes in C-A-S-H composition that can be observed with increasing replacement level, focusing on comparing the calculated K/Si and Na/Si values from mass balance with the measured SEM-EDS values (Figs. 13 and 20). Both sets of results show different trends. The potential reasons for this are described in in section 3.4.5, and as the truth likely lies somewhere in between both sets of results will be discussed. Fig. 20 shows that according to the mass balance there are only minor changes in Na/Si and K/Si with decreasing Ca/Si ratio. According to the SEM-EDS characterization the changes are much larger. With SEM-EDS there is a trend of increasing Na/Si and K/Si with decreasing Ca/Si. Interestingly, the trends look similar to those observed in some studies of synthetic C-A-S-H, such as those from L'Hôpital et al. [14] and Yan et al. [15]. The trends would be even closer in the case that the presently used method of determining Ca/Si underestimates the real ratio for the pastes with FA and VP.

According to the mass balance there is little to no effect on Na/Si and K/Si with increasing replacement level of limestone, FA, or VP (Figs. 13 and 20). According to SEM-EDS, limestone replacement appears to increase both the Na/Si and K/Si ratios. The ratios remained similar for both replacement levels. However, for the cement pastes with FA and VP it appears as though there are effects of increasing replacement level and of temperature, related to the degree of reaction for the pozzolana. Comparing the Na/Si ratios of 25FA-10L to 25FA-10L, there is an almost 5 times increase at both 20 and 38 °C. At 60 °C the Na/Si ratio for 25FA-10L is similar to those of 25FA-10L, potentially as a result of the large increase in degree of VP reaction from 38 to 60 °C (Fig. 6). The same observation is also true for 25FA-10L, which has a comparable Na/Si ratio at 60 °C as those for 25FA-10L. We can conclude from this that although the composite cement pastes with 22 % replacement have more C-A-S-H than at 35 % replacement at 20 and 38 °C, the C-A-S-H at 35 % replacement binds more Na and K per molar unit due to its lower and more variable Ca/Si. This results in the amounts of Na and K bound in C-A-S-H being similar for the composite cements at both replacement levels at 20 and 38 °C. At 60 °C the increased binding comes from both increased amounts of C-A-S-H, and from increased Na/Si and K/Si ratios.

4.3.3. Alkali metals in C-A-S-H

The alkali uptake in the C-A-S-H calculated using the amount of C-A-S-H determined by mass balance with the alkali uptake determined by SEM-EDS is shown in Fig. 21 for all investigated binders. The amounts of Na and K bound by C-A-S-H are plotted as a function of the (Na + K) concentration in the pore solution, resulting in a kind of alkali metal binding isotherm for the different binder systems. This bares similarity to chloride binding isotherms [58]. Hypothetical binding isotherm lines for the investigated binders are included as guides for the eye, following the general shapes of Langmuir (PC and PC-L) and Freundlich (PC-FA and PC-VP) isotherms. Bear in mind that the number of data points are too few and too clustered for us to confidently calculate numbers for the isotherms, so the included lines are only for illustration.

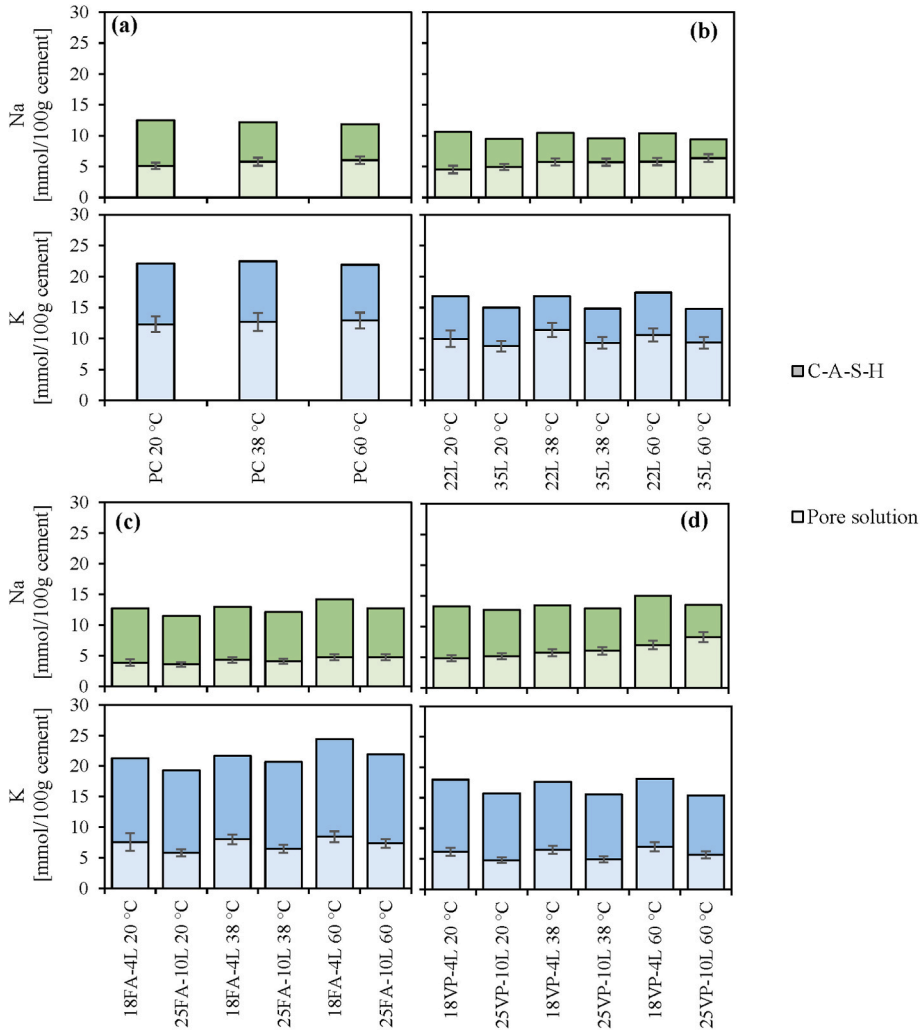

Fig. 19. Na and K released from reacted phases and distributed between C-A-S-H and pore solution according to the mass balance. (a) is the PC pastes, (b) is PC-L, (c) is PC-FA, and (d) is PC-VP.

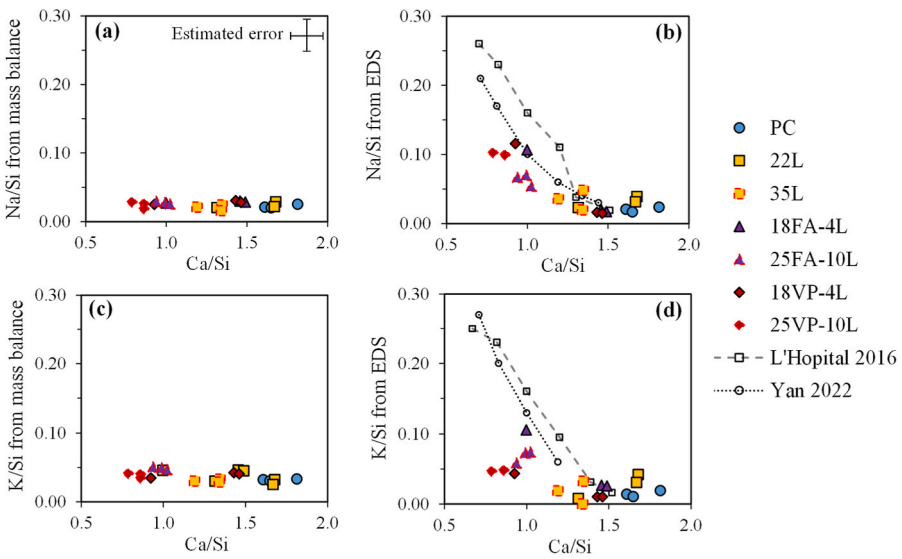

Fig. 20. Na/Si (a and b) and K/Si (c and d) from mass balance (a and c) and SEM-EDS characterization of C-A-S-H in the cement pastes (b and d), plotted against the median Ca/Si ratio of 100–300 SEM-EDS point scans of inner product. Also included are two studies of alkali metal binding in synthetic C-A-S-H, produced with 0.1 mol/L NaOH or KOH [14,15].

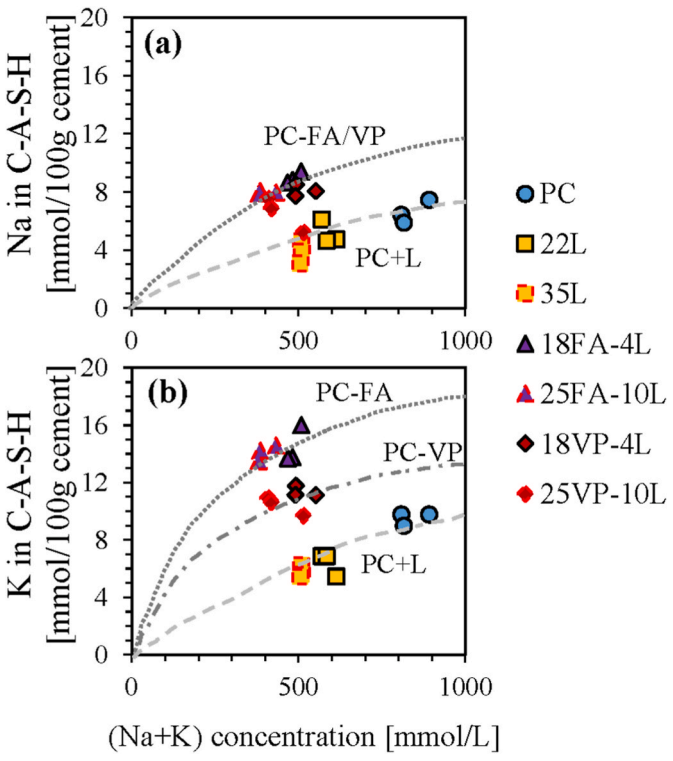

Fig. 21. Changes in the amount of Na (a) and K (b) in C-A-S-H as it varies with the concentrations of (Na + K). Lines are included to represent hypothetical binding isotherms, only included as guides for the eye.

Replacing PC with limestone leads to a reduction in the concentrations of Na and K in the pore solution, as well as the amounts of Na and K in C-A-S-H. Both the PC and limestone system seem to fall on the same isotherm. Limestone seems to have merely a dilution effect but does not drastically change the behaviour of the C-A-S-H, meaning there is simply less of the same C-A-S-H compared to pure PC.

For the cements where PC is replaced with both limestone and pozzolana, the points seem to gather around a different isotherm than the PC and limestone systems. The pozzolans increase the total alkali metal content of the binder, yet simultaneously change the composition of C-A-S-H in ways that increase the alkali metal uptake. This results in a small nett decrease of the alkali metal concentration in the pore solution compared to the limestone containing cement pastes. Our findings agree with those of Chappex and Scrivener [11], where there is a clear difference in alkali metal uptake on C-A-S-H between the composite cement pastes compared to PC and the limestone pastes.

Fig. 21 also illustrates that increasing the replacement level from 18%SCM+4%L to 25%SCM+10%L did not have a large effect on the total alkali metal uptake by C-A-S-H, nor did changes in the curing temperature, as the respective points for the pastes lay rather close to each other.

4.4. Impact for engineering practice

In this study we have tried to understand the impact of increasing replacement levels and curing temperature on the distribution of alkali metals in cement paste. We now wish to discuss some implications of our findings for accelerated performance tests. The scope is limited to relating observations on well-hydrated cement paste to laboratory expansion testing, as the link to field expansion is another actively studied topic.

4.4.1. Are accelerated tests at 38 or 60 °C conservative when testing the impact of increased SCM replacement level?

In principle ASR performance testing of concrete is done at elevated temperatures to accelerate the ASR reaction, or more specifically the dissolution of the aggregate. Curing of concrete at elevated temperatures such as 38 or 60 °C also increases SCM reactivity and can lead to an increase in the DoR of the SCMs. This can potentially lead to an overestimation of the DoR and thereby the mitigating behaviour of the SCM on ASR at ambient conditions. This could render the accelerated test non-conservative.

Based on our findings we are not able to conclude on whether the applied tests are conservative. Monitoring the DoR of the SCM over time at the different temperatures and comparing it to the respective concrete expansion as a potential measure for the aggregate reaction, could have given insight on how the kinetics of both reactions are affected by temperature. But in this study, we only studied the system in depth after 180 days of curing.

4.4.2. To what extent does increasing the SCM replacement level reduce the risk of ASR expansion?

In this study we showed that increasing the replacement level from 22 to 35 wt% led to a decrease in concrete expansion which was linked to a modest decrease in the alkali metal concentration in the pore solution (Fig. 4). The decrease is not proportional to the increase in replacement level, indicating that additional SCM above a certain level has considerably less effect in mitigating ASR expansion. This has been attributed to the limited amount of additional reacted SCM, as large part remains unreacted and serves as a filler.

According to the SEM-EDS results the reduction in the alkali metal concentration upon increasing the SCM replacement level is caused by the enhanced ability of the C-A-S-H to take up alkali metals. It was not caused by the formation of additional C-A-S-H compared to PC as might have been expected, but rather by the (partial) lowering of the Ca/Si in C–S–H, which increases the alkali binding ability of C–S–H and C-A-S-H [14,15].

Whether the additional buffer provided by the changes in the C-A-S-H composition and thereby its ability the take up alkali metals provides a robust mitigation to ASR remains to be seen. Further research is needed to determine how alkali metal uptake in C-A-S-H depends on the C-A-S-H composition with the cement paste and how stable this uptake is. Another important question is how this will vary with the alkali metal concentration. This might be relevant when discussing the effect of leaching, or to exposure of external sources of alkali metals such as NaCl in de-icing salts or salt water.

4.4.3. Is the volcanic pozzolan (VP) a valid alternative for fly ash (FA) at both replacement levels?

Replacing part of the PC with VP reduces the alkali metal concentration in the pore solution in similar way as FA, though the Na concentration is slightly to considerably higher and K concentrations lower than FA. The resulting OH^- concentrations in the FA and VP pastes are similar in both systems. Increasing the replacement level leads to a small additional decrease in the OH^- concentrations. Based on that one could conclude that VP has similar mitigating properties as FA and might therefore be an alternative SCM with respect to ASR mitigation.

Unlike FA, VP contains a large share of non-reactive and unreacted Na. How stable the Na is bound in these phases and whether it over time could be released and potentially contribute to ASR should be further investigated to insure the long-term stability. Additionally, we need to understand whether these phases can react during accelerated tests at higher temperatures. As VP is a natural product one could also expect variations in the content and composition of these phases.

4.5. Further research

The previous study by Hemstad et al. [16] demonstrated how alkali

metals are distributed in composite cement pastes. Now, supplementing with the present study, we got an insight into how increasing the replacement level of PC influences the distribution of Na and K. There are however several questions that remain, both in terms of how to improve the present work and how to apply this knowledge from cement paste chemistry to ASR in concrete.

4.5.1. C-A-S-H characterization

There is still much work to be done to improve characterization of C-A-S-H. This is perhaps the most important step due to the importance of C-A-S-H in the mass balance and its ability to bind alkali metals. Further investigations are needed to bridge the gap between mass balance calculations and SEM-EDS. One approach could be to include NMR for characterization of C-A-S-H.

We also find the recent advances in SEM-EDS characterization reported by Münch et al. [59] and Georget et al. [60,61] to be very promising. In an ongoing follow-up study, we are applying their approach of analysing layered EDS maps to obtain statistical characterization of the C-A-S-H for a selection of the cement pastes investigated in this study. Using this approach, we can move away from discussing C-A-S-H as a single phase with a fixed number for Ca/Si, Al/Ca etc., and rather treat it as a phase with a distribution of these values. Comparing different pastes could be improved if we can report the composition of C-A-S-H in terms of a median or average Ca/Si with a standard deviation and do the same for other relevant ratios like Al/Ca, S/Si, Na/Si and K/Si.

Important in this perspective is also the sample preparation of epoxy-impregnated polished paste sections for SEM-EDS. There is a choice between preparing the sample as is and having the pore solution precipitate on the solids or attempting to remove the pore solution and thereby potentially altering the solids. Neither approach is perfect. Plusquellec et al. [55] showed that one needs solvents consisting of relatively small molecules to extract the alkali metals from paste.

4.5.2. Quantifying reactivity of components

We need improved understanding of how minerals in the SCMs react and potentially release alkali metals to the system. Combined with the reaction degree of the SCMs this is the largest source of uncertainty in the alkali metal balance. This is in part due to the characterization of the raw materials. Na and K are parts of many minor phases, making accurate quantification difficult. These phases are also often minerals with solid solutions, so the exact amount of Na and K in each phase can vary significantly. This issue is very prominent for Na in the pastes with VP. For 25VP-10L at 38 and 60 °C, the uncertainty in the amount of unreacted Na is around the same size as the amount bound in C-A-S-H. The clay-like minerals in limestone could also be a source of alkali metals, and the assumptions that these do not release Na or K should be verified. For cements with a low degree of clinker reaction, it is also important to know how much of the alkali metals remain in unreacted clinker phases. Another important aspect to investigate is whether the curing temperature and pore solution pH influences the reactivity of the individual mineral phases in the SCMs.

A potential solution could be to use SEM-EDS with an automatic mineral system to quantify the types and amounts of minerals in the cement paste before and after hydration. Though, the settings need to be optimized (e.g. lower acceleration voltage) to be able to map the alkali metals.

5. Conclusion

In this study we have investigated how the distribution of alkali metals in hydrated cement pastes change with increasing replacement of PC, and how this influences ASR expansion. Cement pastes with 22 % and 35 % replacement with limestone, fly ash (FA), and a volcanic pozzolan (VP) were cured for 180 days at 20, 38 and 60 °C. The pore solution and solid phases were analysed, and the results were used as input for a mass balance model to determine the phase distribution. Expansion was measured on concrete prisms using the Norwegian concrete prism test (38 °C) and AAR-11 (60 °C) methods.

Replacing PC with only 22 or 35 % limestone did not prevent severe expansion. Replacing 22 or 35 % of PC with FA or VP plus limestone was sufficient to reduce expansion below the acceptance criteria. There appeared to be a threshold concentration of (Na + K) in the pore solution of about 450 mmol/L below which there was no expansion.

The two pozzolans used in this study reduced the (Na + K) concentration of the pore solutions despite bringing more alkali metals to system. A large share of the alkali metals in the SCMs is found in non-reactive minerals and in the unreacted glass-phase, resulting in a similar reactive alkali metal content in the SCM containing cement pastes as in in the reference PC system. Both SCMs considerably reduced the concentrations and total amount of alkali metals in the pore solution compared to limestone replacement.

Increasing the replacement level led to a small reduction in the amount of K in the pore solution but did not affect the amount of dissolved Na. Simultaneously the increase in volume of pore solution at higher replacement levels resulted in a reduction of both the Na and K concentrations in the pore solution. The impact of the replacement level is limited, as the DoR of the SCMs decreases with increasing replacement level, meaning that only a small part of the addition SCM reacts whereas the remaining part acts as a filler.

Replacing parts of PC with pozzolans does not necessarily increase the total mass of C-A-S-H compared to a pure PC paste, but it lowers the Ca/Si ratio which increases the Na/Si and K/Si ratios of the C-A-S-H. Increasing the replacement level of FA and VP decreased the amount of C-A-S-H formed but increased its capacity to bind Na and K, resulting in similar alkali uptake at 22 % and 35 % replacement.

There was a significant discrepancy between the alkali metal adsorption on C-A-S-H as determined by SEM-EDS and by mass balance. The present study is not able to determine which method best represents reality, as both approaches have clear drawbacks.

The curing temperature did not have a considerable impact on the alkali metal concentration in the pore solution for any of the investigated binders, except for the VP containing pastes which due to enhanced reaction showed a higher Na concentration at 60 °C.

Funding

This work was supported by the Norwegian Research Council, Heidelberg Materials Sement Norge AS, Norbetong, Mapei, Rambøll, Skanska, Spenncon, IBRI Rheocenter, the Norwegian Public Roads Administration, and NTNU, through the NEWSCEM project, which had the project number 282578 at the Norwegian Research Council.

CRediT author statement

Petter Hemstad: Conceptualization, methodology, software, formal analysis, investigation, visualization, writing – original draft, writing – review & editing.

Barbara Lothenbach: Supervision, writing – review & editing.

Knut Ose Kjellsen: Supervision, funding acquisition.

Klaartje De Weerdt: Supervision, methodology, project administration, conceptualization, funding acquisition, writing – review & editing.

Declaration of competing interest

The authors declare the following financial interests/personal relationships which may be considered as potential competing interests: Heidelberg Materials provided the raw materials and are intending to produce cement with the volcanic pozzolan provided for this study.Most of this study was performed independently by Petter Hemstad, who was salaried by NTNU during the project and received funding for the experimental work from amongst another Heidelberg.Petter Hemstad

will start working for Heidelberg Materials from the 1st of August 2023.

Data availability

Data will be made available on request. Supplementary data for CCC 2023 publication (Original data) (Mendeley Data)

Acknowledgements

The authors would like to thank Pamela Zuschlag for providing the experimental results from her PhD study. We wish to thank Petter Kjellemyr, Ingrid Masdal, and Steinar Seehus for assistance with experiments. Thank you to Anica Simic, Kyyas Seyitmuhammedov, and Maciej Zajac for performing ICP-OES/MS measurements. Thanks to Ola Skjølsvold, Jan Lindgård, and the team at SINTEF for casting and measuring expansion the concrete prisms. Additional thanks go to Tobias Danner at SINTEF for performing the Rietveld XRD analysis, and Mikael Dissing at DTI for preparing polished sections for SEM-EDS. Finally, thanks to Knut O. Kjellsen, Terje F. Rønning, and Harald Justnes for co-supervising the PhD thesis work of Petter Hemstad.

Appendix A. Pore solution data

Table 6
Pore solution data from ICP-OES/MS.

Cement	Curing temperature °C	Al	Ca	K	Na	S	Si	pH
		mmol/L						–
PC	20	0.43	1.72	631.1	260.4	19.1	0.44	13.63
	38	0.16	1.77	555.9	252.6	62.1	0.29	13.57
	60	0.19	3.00	556.7	258.9	194.9	0.26	13.43
22L	20	0.17	1.78	391.6	177.7	15.5	0.24	13.57
	38	0.09	1.78	408.0	205.7	37.6	0.24	13.56
	60	0.17	2.77	377.8	206.1	127.6	0.26	13.33
18FA-4L	20	0.96	1.63	317.3	164.5	12.3	0.81	13.44
	38	0.59	0.93	303.4	164.4	31.2	0.90	13.42
	60	0.40	1.82	324.2	184.1	112.5	0.55	13.29
18VP-4L	20	0.56	1.13	276.6	214.8	11.1	0.54	13.44
	38	0.48	1.09	260.8	230.4	38.1	0.54	13.37
	60	0.27	2.38	276.6	275.7	141.7	0.42	13.25
35L	20	0.06	1.80	326.1	182.7	8.9	0.19	13.46
	38	0.07	1.79	316.0	193.8	24.2	0.18	13.43
	60	0.08	2.66	300.9	204.1	118.7	0.33	13.19
25FA-10L	20	0.81	0.90	235.6	146.0	8.3	0.69	13.32
	38	0.90	0.84	235.9	149.6	24.2	0.75	13.22
	60	0.46	1.34	261.4	171.5	91.0	0.69	13.12
25VP-10L	20	0.48	0.98	197.0	211.1	11.3	0.62	13.28
	38	0.51	0.95	188.6	229.8	29.6	0.59	13.24
	60	0.28	1.66	209.6	305.4	113.0	0.48	13.17

Appendix B. Quantitative X-ray diffraction

Table 7
QXRD results for the cement pastes.

Cement	Curing temperature °C	C_3S	C_2S	C_3A	C_4AF	CH	Ettringite
		Content in paste [g/100 g cement]					
PC	20	0.4	3.9	0.1	4.9	15.3	2.9
	38	0.0	2.1	0.8	4.9	16.8	2.2
	60	0.5	3.9	1.2	4.9	18.0	2.1
22L	20	0.0	6.4	0.4	2.7	13.5	6.1
	38	0.0	6.2	0.7	3.3	14.5	4.4
	60	0.3	3.5	0.8	4.2	13.6	2.2
18FA-4L	20	0.0	3.6	0.0	3.6	10.2	6.1
	38	0.0	3.8	0.1	4.2	8.6	4.3
	60	1.6	2.6	0.9	4.3	6.1	1.4
18VP-4L	20	1.9	3.2	0.1	2.2	11.7	6.1
	38	2.7	4.4	0.0	4.1	9.6	3.5
	60	2.1	3.3	1.2	3.8	8.3	1.4
35L	20	0.6	2.7	0.8	2.3	11.8	6.4
	38	1.2	3.3	0.6	2.2	12.8	5.9
	60	0.0	3.2	0.9	3.6	11.8	2.8
25FA-10L	20	1.6	2.1	0.5	2.5	7.9	7.5
	38	2.5	1.2	0.7	2.8	7.1	5.4
	60	2.7	0.5	0.9	2.7	3.7	1.6
25VP-10L	20	1.4	1.2	0.4	1.6	6.8	3.9
	38	2.2	1.8	0.4	2.5	6.5	3.1
	60	2.7	2.5	1.2	4.3	6.4	1.2

Appendix C. SEM-EDS

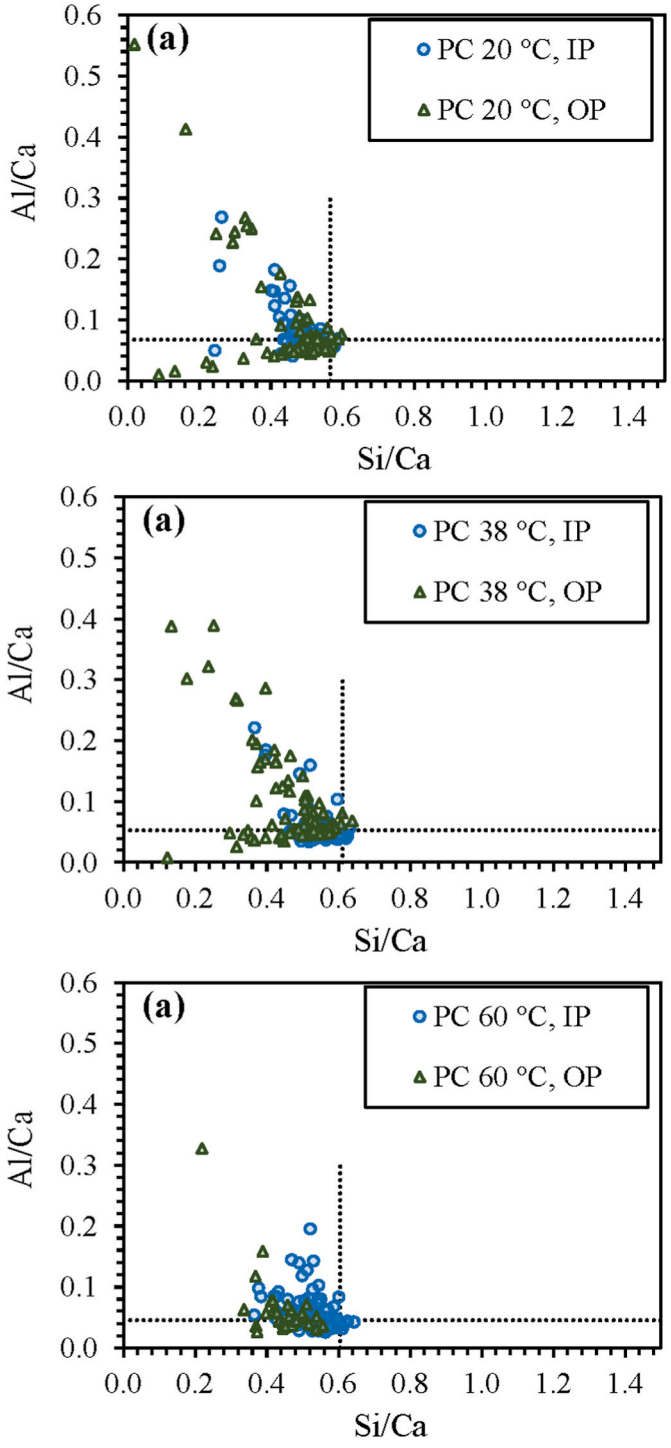

Fig. 22. Al/Ca against Si/Ca scatter plots for the PC pastes.

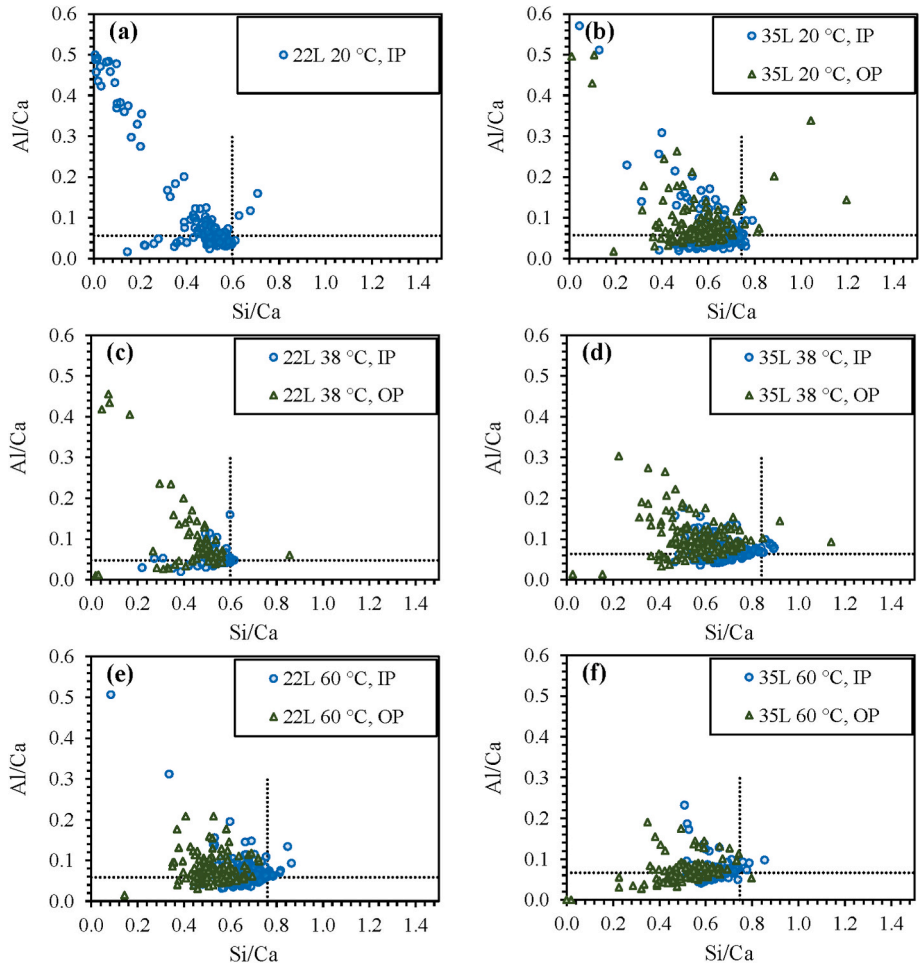

Fig. 23. Al/Ca against Si/Ca scatter plots for the limestone pastes.

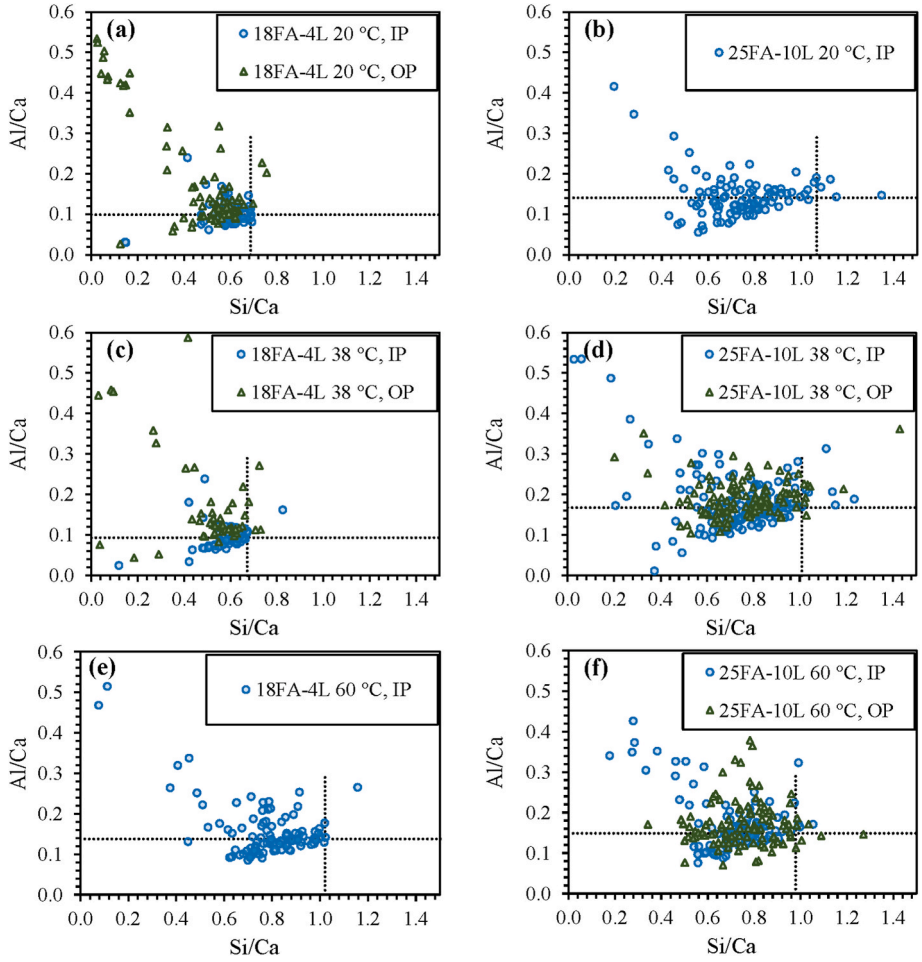

Fig. 24. Al/Ca against Si/Ca scatter plots for the FA pastes.

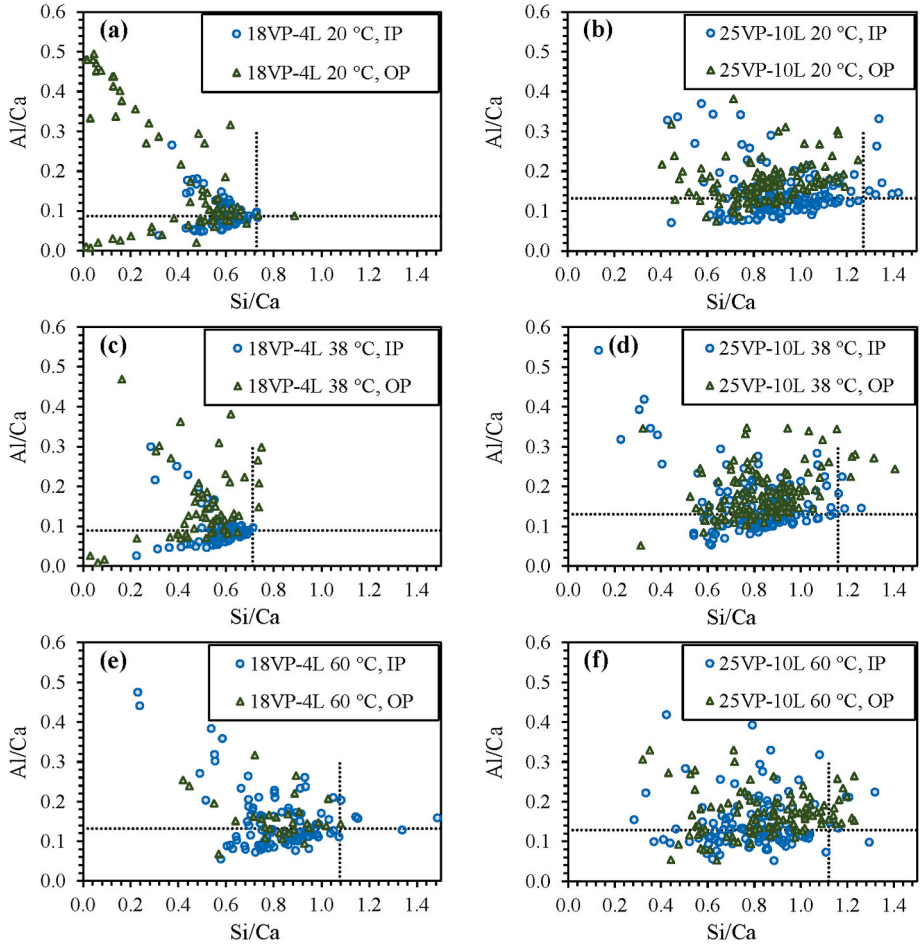

Fig. 25. Al/Ca against Si/Ca scatter plots for the VP pastes.

Appendix D. Supplementary data

Supplementary data to this article can be found online at https://doi.org/10.1016/j.cemconcomp.2023.105344.

References

[1] F. Rajabipour, E. Giannini, C.F. Dunant, J.H. Ideker, M.D.A. Thomas, Alkali–silica reaction: current understanding of the reaction mechanisms and the knowledge gaps, Cement Concr. Res. 76 (2015) 130–146.
[2] S.S. Kongshaug, R.M. Larssen, M.A.N. Hendriks, T. Kanstad, G. Markeset, Load effects in reinforced concrete beam bridges affected by alkali–silica reaction—constitutive modelling including expansion, cracking, creep and crushing, Eng. Struct. 245 (2021).
[3] I. Sims, A. Poole (Eds.), Alkali-Aggregate Reaction in Concrete, A World Review, 2017.
[4] D. Hooton, M.D.A. Thomas, T. Ramlochan, Use of pore solution analysis in design for concrete durability, Adv. Cement Res. 22 (2010) 203–210.
[5] M. Bagheri, B. Lothenbach, K.L. Scrivener, The effect of paste composition, aggregate mineralogy and temperature on the pore solution composition and the extent of ASR expansion, Mater. Struct. 55 (2022) 192.
[6] C. Drolet, J. Duchesne, B. Fournier, Effect of alkali release by aggregates on alkali-silica reaction, Construct. Build. Mater. 157 (2017) 263–276.
[7] P. Rivard, M.A. Bérubé, J.-P. Ollivier, G. Ballivy, Alkali mass balance during the accelerated concrete prism test for alkali–aggregate reactivity, Cement Concr. Res. 33 (2003) 1147–1153.
[8] P. Rivard, M.A. Bérubé, J.-P. Ollivier, G. Ballivy, Decrease of pore solution alkalinity in concrete tested for alkali-silica reaction, Mater. Struct. 40 (2007) 909–921.
[9] W. Chen, H.J.H. Brouwers, Alkali binding in hydrated Portland cement paste, Cement Concr. Res. 40 (2010) 716–722.
[10] H.F.W. Taylor, A method for predicting alkali ion concentrations in cement pore solutions, Adv. Cement Res. 1 (1987) 5–17.
[11] T. Chappex, K.L. Scrivener, Alkali fixation of C–S–H in blended cement pastes and its relation to alkali silica reaction, Cement Concr. Res. 42 (2012) 1049–1054.
[12] S.-Y. Hong, F.P. Glasser, Alkali sorption by C-S-H and C-A-S-H gels, Cement Concr. Res. 32 (2002) 1101–1111.
[13] S.-Y. Hong, F.P. Glasser, Alkali binding in cement pastes Part I. The C-S-H phase, Cement Concr. Res. 29 (1999).
[14] E. L'Hôpital, B. Lothenbach, K.L. Scrivener, D.A. Kulik, Alkali uptake in calcium alumina silicate hydrate (C-A-S-H), Cement Concr. Res. 85 (2016) 122–136.
[15] Y. Yan, S.-Y. Yang, G.D. Miron, I.E. Collings, E. L'Hôpital, J. Skibsted, F. Winnefeld, K.L. Scrivener, B. Lothenbach, Effect of alkali hydroxide on calcium silicate hydrate (C-S-H), Cement Concr. Res. 151 (2022), 106636.
[16] P. Hemstad, P. Zuschlag, P. Kjellemyr, J. Lindgård, K.O. Kjellsen, T.F. Rønning, H. Justnes, K. De Weerdt, Alkali metal distribution in composite cement pastes and its relation to accelerated asr tests (under review), Cement Concr. Res. 173 (2023), 107283.
[17] J. Duchesne, M.A. Bérubé, Effect of supplementary cementing materials on the composition of cement hydration products, Adv. Cement Base Mater. 2 (1995) 43–54.
[18] J. Duchesne, M.A. Bérubé, The effectiveness of supplementary cementitious materials in suppressing expansion due to ASR: another look at the reaction mechanisms. Part 2: pore solution chemistry, Cement Concr. Res. 24 (1994).
[19] M.D.A. Thomas, Supplementary Cementing Materials in Concrete, CRC Press, Boca Raton, FL, 2013.
[20] M.D.A. Thomas, D. Hooton, K. Folliard, Prevention of alkali-silica reaction, in: I. Sims, A. Poole (Eds.), Alkali-Aggregate Reaction in Concrete: A World Review, 2017, pp. 89–118.
[21] Norwegian Concrete Assosiation (NCA/NB) Committee, NB Publication No. 32: Alkali-Silica Reaction in Concrete. Test Methods and Requirements to Laboratories, Oslo, Norway, 2005. (Accessed 11 January 2023).

[22] I. Borchers, J. Lindgård, T.F. Rønning, B.J. Wigum, Recommendation of RILEM TC 258-AAA: RILEM AAR-11: determination of binder combinations for non-reactive mix design or the resistance to alkali-silica reaction of concrete mixes using concrete prisms – 60 °C test method, Mater. Struct. 54 (2021) 203.
[23] T.F. Rønning, B.J. Wigum, J. Lindgård, Recommendation of RILEM TC 258-AAA: RILEM AAR-10: determination of binder combinations for non-reactive mix design using concrete prisms–38 °C test method, Mater. Struct. 54 (2021) 204.
[24] P. Hemstad, Cement Paste Chemistry and its Relation to Concrete Durability. PhD, Trondheim, Norway, 2023.
[25] B. Traynor, H. Uvegi, E. Olivetti, B. Lothenbach, R.J. Myers, Methodology for pH measurement in high alkali cementitious systems, Cement Concr. Res. 135 (2020), 106122.
[26] K.L. Scrivener, R. Snellings, B. Lothenbach (Eds.), A Pratical Guide to Microstructural Analysis of Cementitious Materials, CRC Taylor & Francis, Boca Raton, 2017.
[27] B. Lothenbach, P.T. Durdziński, K. De Weerdt, Thermogravimetric analysis, in: K. L. Scrivener, R. Snellings, B. Lothenbach (Eds.), A Pratical Guide to Microstructural Analysis of Cementitious Materials, CRC Taylor & Francis, Boca Raton, 2017.
[28] P. Zuschlag, The Impact of Curing Temperatures on Portland Composite Cements - Hydrate Assemblage, Porosity, and Compressive Strength, PhD thesis, Trondheim, Norway, 2022.
[29] B. Lothenbach, D. Rentsch, E. Wieland, Hydration of a silica fume blended low-alkali shotcrete cement, Phys. Chem. Earth 70–71 (2014) 3–16. Parts A/B/C.
[30] R.D. Kalina, S. Al-Shmaisani, S. Seraj, R. Cano, R.D. Ferron, M.C.G. Juenger, Role of Alkalis in Natural Pozzolans on Alkali-Silica Reaction, MJ, vol. 118, 2021.
[31] H.F.W. Taylor, Cement Chemistry, Thomas Telford, 1997.
[32] K. De Weerdt, M. Ben Haha, G. Le Saout, K.O. Kjellsen, H. Justnes, B. Lothenbach, Hydration mechanisms of ternary Portland cements containing limestone powder and fly ash, Cement Concr. Res. 41 (2011) 279–291.
[33] A. Vollpracht, B. Lothenbach, R. Snellings, J. Haufe, The pore solution of blended cements: a review, Mater. Struct. 49 (2016) 3341–3367.
[34] F. Deschner, B. Lothenbach, F. Winnefeld, J. Neubauer, Effect of temperature on the hydration of Portland cement blended with siliceous fly ash, Cement Concr. Res. 52 (2013) 169–181.
[35] B. Lothenbach, F. Winnefeld, C. Alder, E. Wieland, P. Lunk, Effect of temperature on the pore solution, microstructure and hydration products of Portland cement pastes, Cement Concr. Res. 37 (2007) 483–491.
[36] B. Lothenbach, T. Matschei, G. Möschner, F.P. Glasser, Thermodynamic modelling of the effect of temperature on the hydration and porosity of Portland cement, Cement Concr. Res. 38 (2008) 1–18.
[37] D. Damidot, F.P. Glasser, Thermodynamic investigation of the CaO-Al2O3-CaSO4-H2O system at 50 °C and 85 °C, Cement Concr. Res. 22 (1992).
[38] R.B. Perkins, C.D. Palmer, Solubility of ettringite (Ca6[Al(OH)6]2(SO4)3*26H2O) at 5–75°C, Geochem. Cosmochim. Acta 63 (1998).
[39] Jeffrey J. Thomas, David Rothstein, Hamlin M. Jennings, Bruce J. Christensen, Effect of hydration temperature on the solubility behavior of Ca-, S-, Al-, and Si-bearing solid phases in Portland cement pastes, Cement Concr. Res. 33 (2003) 2037–2047.
[40] P.T. Durdziński, C.F. Dunant, M.B. Haha, K.L. Scrivener, A new quantification method based on SEM-EDS to assess fly ash composition and study the reaction of its individual components in hydrating cement paste, Cement Concr. Res. 73 (2015) 111–122.
[41] E. Gallucci, X. Zhang, K.L. Scrivener, Effect of temperature on the microstructure of calcium silicate hydrate (C-S-H), Cement Concr. Res. 53 (2013) 185–195.
[42] K. De Weerdt, M. Ben Haha, G. Le Saout, K.O. Kjellsen, H. Justnes, B. Lothenbach, The effect of temperature on the hydration of composite cements containing limestone powder and fly ash, Mater. Struct. 45 (2012) 1101–1114.
[43] K.O. Kjellsen, R.J. Detwiler, O.E. Gjørv, Development of microstructures in plain cement pastes hydrated at different temperatures, Cement Concr. Res. 21 (1991) 179–189.
[44] R. Snellings, A. Machner, G. Bolte, H. Kamyab, P.T. Durdziński, P. Teck, M. Zajac, A.C.A. Muller, K. De Weerdt, M.B. Haha, Hydration kinetics of ternary slag-limestone cements: impact of water to binder ratio and curing temperature, Cement Concr. Res. 151 (2022), 106647.
[45] R.J. Myers, E. L'Hôpital, J.L. Provis, B. Lothenbach, Effect of temperature and aluminium on calcium (alumino)silicate hydrate chemistry under equilibrium conditions, Cement Concr. Res. 68 (2015) 83–93.
[46] X. Zhang, Quantitative Microstructural Characterisation of Concrete Cured under Realistic Temperature Conditions. PhD, Leusanne, Switzerland, 2007.
[47] S. Bahafid, S. Ghabezloo, M. Duc, P. Faure, J. Sulem, Effect of the hydration temperature on the microstructure of Class G cement: C-S-H composition and density, Cement Concr. Res. 95 (2017) 270–281.
[48] F. Avet, K.L. Scrivener, Effect of temperature on the water content of C-A-S-H in plain Portland and blended cements, Cement Concr. Res. 136 (2020), 106124.
[49] K.L. Scrivener, A. Bazzoni, B. Mota, J.E. Rossen, Electron microscopy, in: K. L. Scrivener, R. Snellings, B. Lothenbach (Eds.), A Pratical Guide to Microstructural Analysis of Cementitious Materials, CRC Taylor & Francis, Boca Raton, 2017.
[50] I.G. Richardson, Model structures for C-(A)-S-H(I), Acta Crystallograph. Section B, Struct. Sci. Cryst. Eng. Mater. 70 (2014) 903–923.
[51] I.G. Richardson, J. Skibsted, L. Black, R.J. Kirkpatrick, Characterisation of cement hydrate phases by TEM, NMR and Raman spectroscopy, Adv. Cement Res. 22 (2010) 233–248.
[52] A.V. Girão, I.G. Richardson, R. Taylor, R.M.D. Brydson, Composition, morphology and nanostructure of C–S–H in 70% white Portland cement–30% fly ash blends hydrated at 55 °C, Cement Concr. Res. 40 (2010) 1350–1359.
[53] I.G. Richardson, The calcium silicate hydrates, Cement Concr. Res. 38 (2008) 137–158.
[54] Z. Shi, S. Park, B. Lothenbach, A. Leemann, Formation of shlykovite and ASR-P1 in concrete under accelerated alkali-silica reaction at 60 and 80 °C, Cement Concr. Res. 137 (2020), 106213.
[55] G. Plusquellec, M.R. Geiker, J. Lindgård, J. Duchesne, B. Fournier, K. De Weerdt, Determination of the pH and the free alkali metal content in the pore solution of concrete: review and experimental comparison, Cement Concr. Res. 96 (2017) 13–26.
[56] R. Bleszynski, The Performance and Durability of Concrete with Ternary Blends of Silica Fume and Blast Furnace Slag, PhD, 2002.
[57] M.J. Tapas, L. Sofia, K. Vessalas, P. Thomas, V. Sirivivatnanon, K.L. Scrivener, Efficacy of SCMs to mitigate ASR in systems with higher alkali contents assessed by pore solution method, Cement Concr. Res. 142 (2021), 106353.
[58] P. Hemstad, A. Machner, K. De Weerdt, The effect of artificial leaching with HCl on chloride binding in ordinary Portland cement paste, Cement Concr. Res. 130 (2020), 105976.
[59] B. Münch, L.H.J. Martin, A. Leemann, Segmentation of elemental EDS maps by means of multiple clustering combined with phase identification, J. Microsc. 260 (2015) 411–426.
[60] F. Georget, W. Wilson, K.L. Scrivener, edxia, Microstructure characterisation from quantified SEM-EDS hypermaps, Cement Concr. Res. 141 (2021), 106327.
[61] F. Georget, C. Bénier, W. Wilson, K.L. Scrivener, Chloride sorption by C-S-H quantified by SEM-EDX image analysis, Cement Concr. Res. 152 (2022), 106656.